



HAL
open science

The globus pallidus orchestrates abnormal network dynamics in a model of Parkinsonism

Brice de La Crompe, Asier Aristieta, Arthur Leblois, Salma Elsherbiny,
Thomas Boraud, Nicolas Mallet

► **To cite this version:**

Brice de La Crompe, Asier Aristieta, Arthur Leblois, Salma Elsherbiny, Thomas Boraud, et al..
The globus pallidus orchestrates abnormal network dynamics in a model of Parkinsonism. *Nature Communications*, 2020, 11 (1), 10.1038/s41467-020-15352-3 . hal-03010083

HAL Id: hal-03010083

<https://hal.science/hal-03010083v1>

Submitted on 17 Nov 2020

HAL is a multi-disciplinary open access archive for the deposit and dissemination of scientific research documents, whether they are published or not. The documents may come from teaching and research institutions in France or abroad, or from public or private research centers.

L'archive ouverte pluridisciplinaire **HAL**, est destinée au dépôt et à la diffusion de documents scientifiques de niveau recherche, publiés ou non, émanant des établissements d'enseignement et de recherche français ou étrangers, des laboratoires publics ou privés.

The globus pallidus orchestrates abnormal network dynamics in Parkinsonism

Authors: Brice de la Crompe^{1,2}, Asier Aristieta^{1,2}, Arthur Leblois^{1,2}, Salma Elsherbiny^{1,2}, Thomas Boraud^{1,2}, Nicolas P. Mallet^{1,2*}

Affiliations:

¹ Université de Bordeaux, Institut des Maladies Neurodégénératives, Bordeaux, France.

² CNRS UMR 5293, Institut des Maladies Neurodégénératives, 33076 Bordeaux, France.

*Correspondence should be addressed to nicolas.mallet@u-bordeaux.fr

Keywords: *basal ganglia, abnormal network dynamics, Parkinson's disease, beta oscillations, optogenetic manipulation, motor cortex, subthalamic nucleus, globus pallidus.*

1 **Abstract**

2 The dynamical properties of cortico-basal ganglia (CBG) circuits are dramatically altered
3 following the loss of dopamine in Parkinson's disease (PD). The neural circuit dysfunctions
4 associated with PD include spike-rate alteration concomitant with excessive oscillatory spike-
5 synchronization in the beta frequency range (12-30 Hz). Which neuronal circuits orchestrate
6 and propagate these abnormal neural dynamics in CBG remains unknown. In this work, we
7 combined *in vivo* electrophysiological recordings with advanced optogenetic manipulations in
8 normal and 6-OHDA rats to shed light on the mechanistic principle underlying circuit
9 dysfunction in PD. Our results show that abnormal neural dynamics present in a rat model of
10 PD do not rely on cortical or subthalamic nucleus activity but critically dependent on globus
11 pallidus (GP) integrity. Our findings highlight the pivotal role played by the GP which
12 operates as a hub nucleus capable of orchestrating firing rate and synchronization changes
13 across CBG circuits both in normal and pathological conditions.

14

15 **Introduction**

16 Normal brain functions rely on the overall modulation of cell firing activity and the
17 precise control over the spatiotemporal firing pattern, including (possibly synchronized)
18 oscillatory activity among neuronal network and brain areas ^{1,2}. Disruption in the dynamical
19 properties orchestrating local firing rates and global network oscillations changes are
20 observed in many neurological disorders ³. This is particularly well-illustrated in the basal
21 ganglia (BG) where the loss of dopamine in Parkinson's disease (PD) is associated with
22 persistent alterations in both the firing rate ^{4,5} and oscillatory synchronization among and
23 between BG nuclei ⁶⁻⁸. Defining how these changes interact and are orchestrated is a key
24 aspect to better understand the circuit mechanism underlying their generation.

25 On one hand, spike-rate changes are the backbone of the classic model of BG
26 dysfunction ⁹. In this scheme, dopaminergic loss in the striatum triggers an imbalance in the
27 firing activity of striatal neurons involved in BG direct and indirect pathways, resulting in a
28 cascade of firing rate changes along these circuits which ultimately leads to an over-inhibition
29 of the motor system ^{4,5}. The direct/indirect striatal imbalance in firing activity has been
30 confirmed experimentally ^{10,11}, and the effect of firing rate alterations on the motor deficits in
31 PD is highlighted by optogenetic studies showing that driving hyperactivity in indirect
32 pathway striatal neurons generates a parkinsonian-like state in rodent ¹². In addition, spike-
33 rate features can be predicative of parkinsonism ^{13,14}.

34 On the other hand, changes in BG oscillatory activity are also recognized as a critical
35 functional change associated with PD¹⁵. It materializes as an excessive expression of
36 synchronized oscillatory activity across BG nuclei in the beta (β) frequency range (12-30Hz)
37 in humans or experimental parkinsonism^{16,17}. These synchronized oscillations were first
38 associated with tremors⁷ but seem to be better correlated with akinesia/rigidity^{13,18,19}. Unlike
39 spike-rate changes, their generation mechanisms remain unknown. From a theoretical
40 perspective, any neuronal networks incorporating negative feedback loops with delays can
41 generate oscillatory activity patterns²⁰. The multiple parallel and recurrent inhibitory
42 feedback loops in the BG network include many circuits that, in theory, could generate PD-
43 related β -synchronization²¹⁻²³. The first BG pattern generator system identified was the
44 reciprocally connected subthalamic nucleus (STN) and globus pallidus (GP) circuit^{24,25}. The
45 organization of GP into prototypic and arky pallidal neurons might also constitute a key
46 neuronal substrate to propagate these β -oscillations in BG loop^{26,27}. However, alternative
47 circuit generators have also been proposed in the cortex²⁸, the striatum²⁹, and other BG
48 networks^{21,30,31}. In particular, the cortex is a strong rhythm generator^{32,33} that presents
49 abnormal β -synchronization during PD³⁴. As such, one attractive hypothesis is that the
50 parkinsonian β -oscillations might be generated in the cortex and abnormally
51 maintained/amplified by GP-STN network^{28,35} or the hyperdirect pathway^{23,30}. However, the
52 specific contribution of these different circuit components has never been tested with
53 population-specific and millisecond time-scale control of neuronal networks. In this study, we
54 combined *in vivo* electrophysiological recordings in normal and parkinsonian rats with
55 optogenetic manipulations (i.e. opto-excitation and opto-inhibition) to dissect the specific
56 functional contribution of key cortico-basal ganglia (CBG) components (i.e. the motor cortex,
57 the STN, and the GP) and understand how the generation/propagation of abnormal firing rate
58 and synchronized oscillatory activity in PD is orchestrated.

59

60 RESULTS

61 mCx activity is not necessary for abnormal β -synchronization or STN hyperactivity in 6- 62 OHDA rats.

63 To test the contribution of motor cortex (mCx) in generating abnormal BG network
64 dynamics (including both rate and synchronization changes), we micro-injected an AAV5-
65 CaMKII α (calcium/calmodulin-dependent protein kinase II α)-ArchT3-EYFP virus into both
66 primary and secondary mCx areas of 6-OHDA hemi-lesioned rats (**Figure 1A**). Opto-

67 inhibition of cortical neurons was confirmed using custom-made opto-electrodes (see
68 methods) and extracellular unit recordings (**Figure 1B**). Cortical neurons were all classified
69 as putative pyramidal cells based on action potential duration (**Figure 1C**). Most cortical
70 neurons responded to light stimulation with a significant reduction of firing (**Figure 1D**).
71 Quantitative analysis of the light-induced inhibition both at the individual (**Figure 1E, Table**
72 **S1**) and population level (**Figure 1F**) show that the net effect was an overall strong reduction
73 of mCx neuronal firing rate. We next characterized the impact of mCx opto-inhibition on
74 STN firing and the level of β -synchronization in CBG circuits (**Figure 1G**). These
75 experiments were conducted in an activated cortical state that favors the concomitant
76 expression of both β -oscillations and STN firing hyperactivity^{26,36}. We first showed that most
77 STN neurons decrease their activity during mCx opto-inactivation (**Figure 1H**) but the
78 inhibitory effect was moderate (**Figures 1I, J, Table S1**). Interestingly, STN average firing
79 during mCx opto-inhibition in 6-OHDA rats was still faster than the one recorded in control
80 (i.e. dopamine-intact) animals (**Figure 1I, Table S1**), suggesting that STN firing
81 hyperactivity is not primarily driven by cortical inputs. We then investigated how β -
82 oscillations' expression was affected by mCx opto-inhibition. Looking first at β -oscillations'
83 expression in mCx electrocorticogram (ECoG) power spectrums, we found no effect of mCx
84 opto-inhibition (**Figure 1K**). The first spectral analysis were limited to the best β -oscillations
85 recording epochs (as determined by power, see methods) obtained in each rat. Calculation of
86 the 12-30 Hz β -band areas under the curve (AUC) (**Figure 1L, Table S1**) and measure of the
87 β burst dynamics (**Figures S1A-C**) reveal no significant effect of mCx opto-inhibition. The
88 power of β -oscillations fluctuates *in vivo* between high and low β epoch. To reveal if mCx
89 opto-inhibition had an effect on these dynamical properties of β -oscillations, we quantified
90 the laser effect on each light stimulation by comparing the β -AUC powers ON vs. OFF
91 (**Figure 1M**). To control for the dynamical nature of β -oscillations we also compared the
92 difference between the 2 s β -AUC epoch directly preceding the OFF epochs (i.e. the 'Pre'
93 epoch) and the β -AUC power of the OFF epoch. Interestingly, even when observing
94 individual β epochs of various power, we did not see any significant effect of mCx inhibition
95 on the β -AUC_(OFF-ON) and β -AUC_(Pre-OFF) distribution function (**Figure 1N, Table S1**). Finally,
96 we then investigated if mCx opto-inhibition affected the spike-timing properties of STN
97 neurons during β -oscillations and found that the mean β -phase locking of STN neurons
98 (**Figures 1O and S1D, Table S1**) and the vector lengths (**Figure S1E**) were not significantly
99 impaired by mCx silencing. Although, the β -band coherence between STN unit and mCx
100 ECoG was slightly decreased during mCx inhibition (**Figures S1F, G**), this decrease could be

101 explained by the sensitivity of the spike-field coherence measures to firing rate level ³⁷, as
102 verified by randomly removing action potential in STN spike trains of the same OFF epoch
103 dataset (**Figures S1H-J**). The contribution of other cortical areas (e.g. somato-sensory cortex)
104 in β -oscillations' generation was also **excluded** by performing large-scale cortical ablation in
105 6-OHDA rats (**Figures S2A, B**). Altogether, these results rule out the contribution of mCx as
106 a major source for the generation and the transmission of β -oscillations in the 6-OHDA rat
107 model of PD.

108

109 **STN activity is not necessary for abnormal β -oscillations expression in 6-OHDA rats.**

110 STN neurons are highly synchronized at β frequencies and this activity could be
111 important for orchestrating abnormal β rhythm ^{26,27,38}. We tested the STN contribution to β -
112 oscillations' generation using an opto-inhibitory approach (**Figure 2A**) based on two different
113 viral constructs: either an AAV5-CaMKII α -eArchT3-EYFP virus as performed in a seminal
114 study ³⁹, or an AAV5-hSyn-eArch3-EYFP that contain a ubiquitous and neuron-specific
115 promotor: the human synapsin 1 (hSyn). Qualitative (**Figure 2B, C**) and quantitative (**Figures**
116 **S3A, B**) **histological** control of EYFP expression confirms the transduction of STN neurons
117 and appropriate axonal labelling in STN target regions for both viral approaches. The efficacy
118 of STN opto-inhibition was verified for each animal using opto-electrode mapping and the
119 animals that did not reach satisfactory level of STN inhibition (i.e. >60%) were excluded from
120 further analysis (see methods). For both sets of experiments, STN neuronal firing rate was
121 strongly reduced by light stimulation (**Figures 2D, E, Table S2**). We next tested the impact of
122 STN opto-inhibition on the expression of β -oscillations (best β -power recordings for each rat).
123 **We found that the β power (Figure 2F, Table S2) and the β burst duration (Figures S3C)**
124 **were not affected by STN opto-inhibition whereas the β burst count was slightly decreased**
125 **(Figure S3D).**To analyze if STN opto-inhibition had an effect on β dynamics, we next
126 compared all the individual β epochs in control vs. laser conditions and found either no laser
127 effect in CaMKII α -eArchT3-STN (**Figure 2H, Table S2**) or a small reduction in the hSyn-
128 eArchT3-STN group (**Figure 2H, Table S2**). We also performed GP LFPs recordings in
129 hSyn-eArchT3-STN rats to identify if β -synchronization was affected in BG circuits. We
130 found that although the coherence between GP LFPs and mCx ECoG was significantly
131 reduced (**Figure 2I, Table S2**) it was nevertheless not suppressed by STN opto-inhibition.
132 **The lack of strong effects on β dynamics consequent to STN opto-inhibition was further**
133 **confirmed by the results of STN ablation. Indeed, we found that electrolytic lesion of the STN**

134 did not affect the level of β -oscillations expression in lesioned rats (**Figures S4A, B**). In
135 conclusion, our data reveal that, against the current assumption, STN activity in 6-OHDA rats
136 is not involved in the generation of abnormal β oscillations and, at best, only play a supportive
137 role.

138

139

140 **Opto-patterning of STN neurons at β frequency does not replicate the functional**
141 **properties of abnormal β -oscillations in normal rats.**

142 The inability to fully suppress the activity of all STN neurons during our opto-
143 inhibition protocol could, in theory, explain the absence of visible effect on β -oscillation
144 expression. To further test if STN neurons are important for β generation, we artificially
145 introduced β -oscillations directly at the level of STN in normal animals and dissected the
146 functional properties and neuronal substrates of these synthetic β -oscillations in comparison
147 to the parkinsonian β recorded in 6-OHDA rats. Reverse engineering of β -oscillations was
148 achieved by directly patterning the activity of STN neurons at β frequency (20 Hz) using an
149 optical excitatory (AAV-CaMKII α -ChR2(H134R)-EYFP, **Figures 3A, B**) or an inhibitory
150 approach (AAV-CaMKII α -eArchT3.0-EYFP, **Figures S5A, B**). These excitatory/ChR2 and
151 inhibitory/ArchT3.0 β -patterning strategies were also used to dissect the functional
152 contribution of specific excitatory vs. inhibitory inputs to STN neurons. We first validated
153 these tools using opto-electrode mapping in STN. As expected, opto-patterning STN neurons
154 at β frequency artificially synchronized STN neurons activity at 20Hz (**Figures 3E, S5F**) and
155 this activity could propagate to generate abnormally high level of cortical β -oscillations
156 (**Figures 3C, S5D, Table S3**) and cortico-STN coherence (**Figures S6A, B**). Interestingly,
157 these STN opto-patterning protocols were more efficient at generating abnormal β
158 synchronizations (as measured in the ECoG) when the brain state of the animal was activated
159 as opposed to slow-wave oscillations. This property parallels the brain-state dependency of
160 parkinsonian β -oscillations expression already described in anaesthetized²⁶ and awake³⁶ 6-
161 OHDA lesioned rats. As such, these opto-patterning experiments were preferentially
162 performed in an activated brain state. Combining STN-ChR2 β -patterning with unit activity
163 recordings of the two main population of GP neurons (i.e. the prototypic and arkypallidal
164 cells) also reveal that synthetic β -oscillations could propagate to GP neurons and cause a
165 significant increase in the temporal coupling (measured through coherence analysis) between
166 cortex and the two populations of GP neurons (**Figures S6A, B**). We next assessed if our

167 synthetic β -synchronization shared the same **or as many as possible** functional properties as
168 parkinsonian β -oscillations. In particular, we focused our analysis on the known STN/GP
169 neurons spike-timing **properties during these oscillations (that is the** antiphase relationship
170 between STN/prototypic **and prototypic/arkypallidal neurons, as well as the** in-phase
171 relationship between STN/arkypallidal neurons ^{26,27}) **and the associated firing rate changes**
172 **(that is the hyperactivity of STN neurons vs. the decrease firing of prototypic neurons).**
173 Importantly, these fine STN/GP spike-timing **features during** PD β -oscillations were
174 confirmed in our dataset (**Figure 3D**). On the contrary, artificial **ChR2-induced** β -oscillations
175 did not reproduce **any of** the correct STN/GP phase-locking preferences (**Figure 3E, Table**
176 **S3**) **while ArchT3.0-induced β -oscillations reproduced the correct phase-locking value of**
177 **STN neurons but not the one of GP (Figure S5F).** Importantly, both these artificial β -
178 oscillations did not replicate the stereotypical antiphase firing relationship between STN and
179 prototypic GP neurons (**Figures 3D, S5F, G**). Instead, we found that the phase lags between
180 STN and prototypic neurons ($\sim 57^\circ$ for ChR2, **Figures 3E** vs. $\sim 42^\circ$ for ArchT3.0, **Figures**
181 **S5G**) represent a time delay of 7.9 ms **and 5.8 ms, respectively,** compatible with a
182 monosynaptic excitatory drive from STN inputs to prototypic neurons ⁴⁰. Interestingly though,
183 **in both cases,** we could reproduce (albeit with different phase-locking values toward the
184 cortical β -cycle reference) the antiphase relationship between prototypic and arkypallidal
185 neurons (**Figures 3D, E and S5G**) suggesting that this opposition of phase **is likely** driven by
186 prototypic neurons collateral inhibition onto arkypallidal cells. These firing relationships
187 between STN/GP neurons were also confirmed using longer (2 s) continuous light stimulation
188 **in the ChR2 dataset (Figures S6C-E).** Finally, considering firing rate changes induced by the
189 **ChR2 or the ArchT β -patterning,** we found that, **in both cases,** artificial β -oscillations could
190 not faithfully reproduce the rate changes associated with parkinsonian β -oscillations (**i.e.** STN
191 hyperactivity and prototypic neurons hypoactivity ^{26,27}). Indeed, here **ChR2** opto-patterning of
192 STN neurons at β frequency reproduced STN increase firing (**Figure 3F, Table S3**) but also
193 induced hyperactivity of prototypic cells (**Figure 3F, Table S3**), **whereas ArchT3.0 reduced**
194 **cell firing in both STN and GP neurons (Figure S5H).** Taken altogether, these results obtain in
195 lesioned and control animals invalidate the causal importance of STN neurons in driving
196 abnormal BG network dynamics in PD rodents **from specific excitatory or inhibitory inputs.**
197
198

199 **GP Opto-inhibition suppresses abnormal β -synchronization in CBG loop in 6-OHDA**
200 **rats.**

201 The dichotomous organization of the GP into prototypic and arky pallidal neurons has
202 been proposed as a key neuronal substrate in PD to maintain and propagate abnormal β -
203 synchronization to the whole BG circuit ²⁷. To test if GP activity was important for β -
204 oscillations expression, we applied a global opto-inhibition approach using an AAV5-hSyn-
205 eArch3-EYFP virus. Histological verification of the reporter EYFP protein confirms the
206 transduction of GP neurons as shown by the dense axonal labelling in STN and substantia
207 nigra pars compacta (SNc) and SNr (**Figure 4A**). We next verified the laser inhibitory effect
208 and spread in GP using an opto-electrode made of 2 optic fibers (placed at 1, or 2 mm from
209 the recording tip). Prototypic and arky pallidal neurons were identified through their
210 distinctive electrophysiological signature (**Figure 4B**)^{27,41}. Extracellular *in vivo* recordings
211 showed that most putative prototypic neurons were significantly inhibited by light stimulation
212 placed at 1 mm (**Figures 4C-E, Table S4**) or 2 mm above the recording electrode (**Figures**
213 **S7A, C**). Putative arky pallidal neurons were also strongly inhibited by light stimulation both
214 from the 1 mm (**Figures 4D, F, Table S4**) or 2 mm spaced fibers (**Figures S7B, D**). Overall,
215 these *in vivo* GP recordings confirm that our opto-stimulation had a strong and global
216 suppressive effect on both GP neuronal populations. We next assessed the functional impact
217 of GP opto-inhibition onto STN firing activity and mCx ECoG during abnormal β -
218 synchronization (**Figure 4G**). We first found that GP opto-inhibition produced a strong
219 excitatory response in most STN neurons (**Figures 4H-J, Table S4**), highlighting the
220 powerful tonic inhibitory control exerted by prototypic GP neurons onto STN activity.
221 Similarly, β power analysis in mCx ECoG during GP opto-inhibition revealed a strong
222 suppression of β -oscillations expression (**Figure 4K**). Both β -AUCs computed on the best β
223 recordings (**Figure 4L, Table S4**) and on all individual β epochs (**Figures 4M, Table S4**)
224 were significantly reduced in laser vs. control conditions. **The β burst dynamics (i.e. duration**
225 **and counts) were also strongly disrupted (Figures S7I, J)**. Furthermore, at the population
226 level, the STN β phase-locking histogram was strongly suppressed by GP opto-inhibition
227 (**Figure 4N**). At individual neuronal level, all phase-locked STN neurons had a significant
228 decrease in their vector lengths value (**Figures S7E, F**) and their strength of entrainment
229 (only 9 out of the 35 phase-locked neurons were still significantly entrained with a Rayleigh
230 test value $p < 0.05$). Also, STN spike-field coherence measures (using mCx ECoG as field)
231 were significantly suppressed by GP opto-inhibition (**Figures S7G, H**). In conclusion, our

232 results strongly support the idea that GP activity is important and required for the generation
233 of β -synchronization in 6-OHDA rats.

234

235 **Change in the dynamical state of STN neurons firing rate do not cause β -**
236 **synchronization suppression in 6-OHDA rats.**

237 How changes in firing rate impact neuronal synchronization is unclear. It is thus
238 possible that the strong increase in STN firing caused by GP disinhibition, impairs the
239 entrainment capacity of STN neurons (i.e. single-cell level effect) or, alternatively, provides a
240 profound change in the excitatory state of the whole BG circuit (i.e. network level effect) that
241 might indirectly contribute to β -synchronizations disruption. To account for both these
242 possibilities, we tested two approaches aimed to either mimic the increase of STN firing rate
243 either at the single-cell level (i.e. juxtacellular approach) or at the network level (i.e. opto-
244 excitation of STN). Juxtacellular stimulation of STN neurons using current injection (**Figure**
245 **5A**) was sufficient to significantly increase the firing activity of single STN neurons during β
246 synchronization (**Figure 5B**). The intensity of current injection was adapted for each STN
247 neuron to induce a sufficient excitation level (**Figure 5C, Table S5**). Quantification of STN
248 neurons' frequency modulatory index (MI) showed that the excitatory effect induced by
249 current injection was similar (albeit slightly higher) than the one obtained following GP opto-
250 inhibition (**Figure 5D, Table S5**). Such depolarization, at the single cell level, did not affect
251 the capacity of STN neurons to be phase-locked to β -oscillations (**Figure 5E, Table S5**).
252 Indeed, all excited STN neurons were still entrained by β -oscillations during the ON-
253 juxtacellular epochs with no effect on the mean phase angles (**Figure S8A**) and a slight
254 diminution of the vector lengths (**Figure S8C**). Also, the β -band coherence between STN unit
255 and mCx ECoG was significantly increased during juxtacellular stimulation (**Figures S8E,**
256 **G**), and this effect was likely due to the increase in the firing rate (see **Figure S1I**). To test if
257 a global change in BG network dynamical state was responsible for β synchronization
258 disruption, we performed global STN opto-excitation (**Figure 5F**). Qualitative histological
259 observation (**Figure 5G**) revealed sufficient STN transduction while our *in vivo* recordings
260 confirmed the excitatory effect on STN neurons (**Figure 5H**). We could thus reproduce using
261 opto-stimulation an overall level of STN excitation similar to the one obtained with GP
262 silencing (**Figure 5I**) and the change in MI were not statistically different in both conditions
263 (**Figure 5J, Table S5**). This strong increase in STN excitatory drive did not impair, nor boost
264 β -oscillations power in mCx (**Figure 5K, Table S5**). The β -phase locking of STN neurons
265 was slightly shifted to early phases (**Figure 5L, Table S5**) but most STN neurons were still

266 significantly entrained by β -oscillations (n=23/27, Rayleigh test $p<0.05$) with a small decrease
267 of both mean phase angles (**Figure S8B**) and vector lengths (**Figure S8D**). The β -band
268 coherence between STN unit and mCx ECoG was not affected by light stimulation (**Figures**
269 **S8F, H**). These results support the idea that β -oscillations suppression following GP opto-
270 inhibition was not caused by a dynamical change in STN excitatory state but rather due to the
271 loss of GP contribution in orchestrating β -rhythm across CBG circuits.

272

273 **Opto-patterning of GP neurons at β frequency generates β -oscillations with similar** 274 **functional properties as rodents' parkinsonian β -oscillations.**

275 During natural β -oscillations, the tonic firing activity of prototypic neurons is strongly
276 decreased as compared to control animals^{27,42} despite receiving more excitation from a
277 hyperactive STN³⁶. In addition, GABAergic D2-MSNs neurons, which increase their activity
278 following DA loss¹⁰, become selectively entrained at β frequency⁴³. These data suggest that
279 inhibitory striatal inputs rather than STN excitation might shape GP abnormal neuronal
280 dynamics (i.e. decrease in firing rate and β -synchronization). We tested this hypothesis using
281 an opto-inhibitory patterning strategy to artificially introduce β -oscillations at the level of GP
282 neurons (**Figure 6A**). The injection of AAV5-hSyn-eArch3-EYFP virus was performed in the
283 GP of normal rats and confirmed by histological verification (**Figure 6B**). Rhythmic
284 optogenetic inhibition of GP neurons at 20Hz induced β -oscillations expression in mCx
285 (**Figure 6C, Table S6**) and increase β frequency coherence of STN/GP neurons toward mCx
286 (**Figures S9A, B**) which was due to strong β -phase locking of STN/GP neuronal populations
287 (**Figure 6E**). **As previously, we** compared the spike-timing relationship and phase-locking
288 values induced by this synthetic β (**Figure 6E, Table S6**) with parkinsonian β (**Figure 6D,**
289 **Table S6**) for prototypic, STN and arky pallidal neurons. In contrast to the results obtain with
290 the STN β -patterning, we found here that the phase-locking values of prototypic and STN
291 neurons towards synthetic cortical β -oscillations were similar to the one measured in 6-
292 OHDA rats. Importantly, we could also reproduce the antiphase relationship typically present
293 between prototypic and STN neurons in PD condition, suggesting that STN β -synchronization
294 is shaped as a consequence of GP prototypic activity and not the reverse. **However, unlike our**
295 **previous STN opto-patterning experiments, GP opto-inhibition did not reproduce the**
296 **opposition of phase classically present between arky pallidal and prototypic neurons during β -**
297 **rhythm. This was likely caused by the fact that our GP inhibitory effect was global and**
298 **affected both the activity of arky pallidal and prototypic neurons. This finding hints towards**

299 the possibility that the inhibitory inputs shaping the parkinsonian β -oscillations preferentially
300 impact onto prototypic neurons (as did STN inputs) and not arkyvallidal neurons. In addition,
301 considering firing rates, these β -pattern optogenetic manipulations of GP reproduced the
302 directional firing rate changes classically described in prototypic and STN neurons during
303 parkinsonian β -oscillations, that is: a significant decrease in prototypic activity and a
304 significant increase in STN activity. The inhibitory influence of GP neurons on STN firing
305 was also evident using longer (2 s) and continuous light stimulation (**Figure S9C**). Indeed, as
306 in 6-OHDA lesioned rats, the baseline STN firing rate level in control animals was strongly
307 dependent upon GP activity (**Figures S9D, E**). These experiments also reveal the existence of
308 an inverse correlation between the baseline firing rate of STN neurons (i.e. Frequency OFF)
309 and the disinhibition amplitude induced by GP opto-inhibition (**Figure 6G**). Interestingly, this
310 correlation was weaker in PD rats as compared to control animals (**Figure 6G, Table S6**),
311 thus arguing that the control of STN neurons firing rate by GP neurons was partly occluded in
312 6-OHDA lesioned animals as evinced by the higher baseline firing of STN neurons.
313 Altogether, these results show that the generation of abnormal β -synchronization requires a
314 state of increase incoming inhibition to GP prototypic neurons and that prototypic neuronal
315 activity plays a key role in controlling firing rate level and orchestrates neuronal
316 synchronization in STN neurons in both normal and pathological conditions.

317

318 **Discussion:**

319 In this work, we used optogenetic stimulation, which provides fast, reversible, and
320 population-selective neural manipulation to shed light on the functional contribution of mCx,
321 STN and GP to the expression of CBG neural dynamics in control and hemi-parkinsonian
322 rodents.

323

324 **Cortical activity is not necessary to generate parkinsonian β -oscillations**

325 One influential hypothesis suggests that β -oscillations are generated from cortical
326 sources in normal and pathological conditions, which then propagates to BG circuits (i.e.
327 particularly through the cortico-STN ‘hyperdirect’ pathway) where they become abnormally
328 amplified in parkinsonism to reach pathophysiological levels⁴⁴. Functional coupling analyses,
329 applied to data recorded from PD patients^{45–48} and animal models of parkinsonism⁴⁹ have
330 shown that cortical β -oscillations precede in time STN abnormal oscillatory activity, arguing
331 for a cortical drive. However, such phase-differences analyses might not necessarily vouch for

332 causal interactions. Here, we directly tested the cortical β -generation hypothesis using
333 widespread mCx opto-inhibition in a rat model of PD (Figure S10A). We found that mCx
334 inactivation or large-scale cortical ablation did not alter the level of abnormal β -oscillations
335 expression in CBG circuits. Opto-inhibition of mCx also had a weak effect on STN firing rate
336 hyperactivity which is not entirely surprising. First, STN neurons have autonomous
337 pacemaker firing properties⁵⁰, and there is good evidence that the cortico-STN transmission
338 is profoundly reduced in both rodent and monkey PD models^{51,52}. The capacity of
339 parkinsonian β -rhythm to synchronize BG circuits in a cortex-independent manner could
340 therefore represent a novel pathological feature of these oscillations. Indeed, if cortical
341 activity can no longer control spike-rate and synchronization changes in BG circuits, this
342 could certainly impair the information processing flow, leading to functional deficits. Re-
343 establishing cortical control over BG activity might restore some level of functionality in
344 these circuits and could potentially explain the reduction of parkinsonian signs observed
345 following cortical deep brain stimulation^{34,39,53}. Altogether, our results argue against a
346 cortical origin of parkinsonian β -oscillations and rule out a significant contribution of the
347 hyperdirect pathway in driving STN hyperactivity or β -oscillatory activity⁵⁴. Importantly
348 though, these results do not exclude the possibility that the spontaneous and transient β -
349 oscillations classically recorded in dopamine-intact conditions during movements are
350 generated through cortical mechanisms⁵⁵⁻⁵⁸. Indeed, it remains to be addressed whether
351 parkinsonian β -oscillations originate from dysregulation in space and time of normal β -
352 oscillations^{59,60} or whether they are generated through entirely different circuit mechanisms.

353

354 **STN neurons are not necessary for parkinsonian β -oscillation synchronization**

355 The STN firing-rate increase and synchronized β -oscillatory activity represent a
356 stereotypical hallmark of parkinsonism^{36,38,61}, and these changes could contribute to a
357 stronger functional impact of STN neurons onto CBG activity in the PD state³⁸. In addition,
358 the STN is reciprocally-connected to GP neurons⁶² and this microcircuit forms a negative
359 feedback loop that has been proposed to generate²⁴, amplify²⁵, or propagate synchronized
360 oscillatory activity *in vivo*²⁶ (Figure S10B). The intrinsic properties of STN neurons could
361 also reinforce abnormal oscillatory activity through post-inhibitory rebound activity^{63,64}.
362 However, we show here that STN opto-inhibition, opto-excitation, and lesion had very limited
363 effect on parkinsonian β -oscillation expression. In addition, reintroducing β -oscillations
364 directly at the level of STN in normal animals (using β -frequency opto-patterning) did not

365 mirror the firing rate alterations measured in GP prototypic and arkyallidal neurons in
366 parkinsonian rats⁴². Furthermore, it did not reproduce the correct spike-timing relationships
367 classically observed in the PD condition between STN neurons, prototypic, and arkyallidal
368 neurons²⁶. Instead, the phase relationships we obtained when opto-exciting or opto-inhibiting
369 STN inputs are consistent with a preferential functional impact onto prototypic neurons
370 (causing an in-phase relationship with STN), and an opposite response in arkyallidal neurons
371 (causing an anti-phase relationship) likely driven by disynaptic inhibition. The excitatory
372 response induced in prototypic neurons upon STN activation has a short synaptic delay (<6
373 ms) compatible with a direct monosynaptic STN drive⁴⁰, whereas arkyallidal inhibition is
374 likely driven by prototypic axon collateral²⁷. Such preferential integration of excitatory STN
375 inputs onto prototypic vs. arkyallidal neurons could reflect a differential synaptic
376 organization of STN inputs and/or a difference in collaterals inhibitory balance between the
377 two populations of GP neurons. It is tempting to speculate that the differences of spike-timing
378 in STN/GP network during parkinsonian β vs. artificial β -oscillations could be due to a
379 reorganization of STN axonal connectivity onto GP neurons induced by the lack of dopamine
380 which can trigger many adaptive changes affecting the functional connectivity within CBG
381 circuits^{51,65-67}. However, the anti-phase activity of GP prototypic neurons and STN neurons
382 present after dopamine lesions is also observed in dopamine-intact animals during
383 synchronous spike-and-wave discharges that underlie absence epileptic seizures⁶⁸. This
384 suggests that the temporal structure of STN/prototypic spike interactions during abnormal
385 synchronized oscillations is imposed by GP prototypic inhibitory activity and not by STN
386 excitatory drive. Altogether, these results cast doubt on the capacity of STN neurons to
387 generate, propagate or amplify abnormally synchronous oscillatory activity at β -frequency in
388 CBG circuits in a rodent model of PD.

389

390 **GP activity orchestrates abnormal network dynamics in basal ganglia circuits**

391 The functional importance of GP neurons has dramatically changed in the past two
392 decades from being a simple relay nucleus in the indirect pathway^{5,69} to being a central and
393 integrative hub within BG circuits^{70,71}. In the PD pathological state, the dichotomous
394 organization of GP neurons has been proposed to play a key role in coordinating and
395 broadcasting pathological network activity^{26,27,72} (Figure S10C). Here, we demonstrate for
396 the first time that GP activity is indeed necessary for the expression and propagation of
397 abnormal β -oscillations in a rodent model of PD. We also show that GP prototypic neurons

398 control baseline STN firing activity both in control and PD conditions. This strong and tonic
399 inhibitory influence likely extends to other nuclei both within and outside BG, especially
400 considering the diverse and widespread projections of GP neurons^{27,73,74}. Interestingly
401 though, the disinhibitory effect induced in STN by GP opto-inhibition was smaller in PD as
402 compared to control animals. These differences could be due to the decrease in prototypic
403 neuronal firing in the PD state that contributes to STN hyperactivity and may thus partially
404 occludes the disinhibition induced by GP opto-inhibition. As such, the synaptic adaptation
405 that has been described for prototypic neurons (i.e. increase strength and number of synapses
406 in STN)^{66,75} might thus be a compensatory phenomenon to maintain effective inhibition onto
407 STN neurons. The origin of the prototypic firing rate decrease observed during β -oscillations
408 is an important question. Given the hyperactivity of STN induced by DA-loss and that it
409 preferentially excites prototypic neurons, the most likely cause of prototypic firing reduction
410 is the concurrent increase in inhibition coming from striatal indirect projection neurons^{10,11,43}.
411 Striatal indirect neurons become selectively entrained during β -oscillations⁴³ with a phase
412 preference that precede STN activity by 45° (which corresponds to ~ 6 ms assuming a 50 ms
413 β -cycle period)²⁶ so striatal β -inhibition and STN β -excitation will hit the GP at around the
414 same time. The total number of striatal neurons far exceed those in STN⁷⁶ and this is also true
415 for the number of synaptic contacts established in the GP^{77,78}. Considering these figures, the
416 synaptic ratio of striatal vs. STN inputs is ranging from 30:1 to 50:1, supporting the idea that
417 GP activity might be primarily controlled by striatal inhibition during excessive neuronal
418 synchronization. We confirm here that rhythmic inhibition of GP neurons reproduces the
419 correct spike-timing and firing rate relationship classically measured during parkinsonian β -
420 oscillations between STN and prototypic neurons. The importance of increased striatal
421 inhibition to induce abnormal oscillatory activity in GP has been suggested by many
422 computational studies^{79,80} but how this increase leads to the generation of synchronization at
423 β -frequency is not currently clear. One possibility is that increased striatal inputs trigger a
424 switch of GABAergic control within GP from a state dominated by local collateral inhibition
425 that favor GP decorrelated firing mode^{81,82} to a state driven by striatal inputs that favor GP
426 neuronal correlations. The contribution of arky pallidal neurons, which send dense inhibitory
427 projections onto striatal neurons^{27,41}, or the projections from a subpopulation of prototypic
428 neurons that selectively contact striatal GABAergic interneurons⁸³ could further promote the
429 amplification of β -synchronization³¹.
430

431 **Conclusion on the circuit mechanisms generating β -oscillations**

432 Whether β -oscillations are an emerging property of the striatum ²⁹, the striatal-GP
433 microcircuit, or a larger feedback loop that includes the thalamus ⁸⁴ is not known but will be
434 important to address in future experiments. Another important aspect would be to determine if
435 similar circuit mechanisms apply to the generation of abnormal β -synchronization in PD
436 primates. Indeed, correlation analyses have shown that β -synchronization in primate GP
437 seems to be principally driven by STN and not striatal activity ³⁸. In addition, the STN
438 appears to be necessary for the expression of β -oscillations in MPTP-treated monkeys ^{35,85}.
439 The contribution of the striatum is less clear: blockage of GABA transmission in the GP does
440 not affect/suppress β -oscillatory activity ^{35,85} and, despite the reduction of GP activity in
441 MPTP primate as compared to control animals ³⁸, there is still some debate as to whether
442 striatal activity is increased ^{86,87} or not ³⁸. Altogether, our data draws strong and testable
443 predictions that might help in resolving these issues. Indeed, if STN activity drives β -
444 synchronization in primates, then STN activity should have an ‘in-phase’ relationship with the
445 main population of GP neurons (i.e. the prototypic). We show here however that the scenario
446 leading to the generation of abnormal β -oscillations dynamics in PD rodents is different and
447 principally relies on inhibitory mechanisms that are orchestrated and broadcasted to the CBG
448 network by GP neurons.

449

450 **Acknowledgements:** This work was supported by grants from the French Agence Nationale
451 de la Recherche (ANR-14-CE13-0024-01 and ANR-15-CE37-0006), from the CNRS PEPS
452 Idex Bordeaux (UB101 CR-2014R), and the LABEX BRAIN ANR-10-LABX-43. B. de la
453 Crompe was supported by a fellowship from French Ministry (Higher Education, Research
454 and Innovation), from France Parkinson nonprofit organization (UB320 CR-3219R), and from
455 the LABEX BRAIN (UB106 CR-3219R). We are grateful to Dr. Hansel, and Dr. Magill for
456 insightful scientific discussions; Dr. Deffains, Dr. Baufreton, and A. McDonald for comments
457 on the manuscript. The authors declare no competing financial interests.

458

459 **Author Contributions:** Conceptualization, B.C., T.B., and N.M.; Methodology, B.C., A.A.,
460 and N.M.; Formal Analysis and Software, B.C., A.L., and N. M.; Investigation, B.C., A.A.,
461 S.A. and N.M.; Writing – Original Draft, B.C.; Writing – Review and Editing, N.M.; Funding
462 Acquisition, N.M.; Resources and Supervision, N.M.

463 **Declaration of Interests:** The authors declare no competing interests.

Figure 1

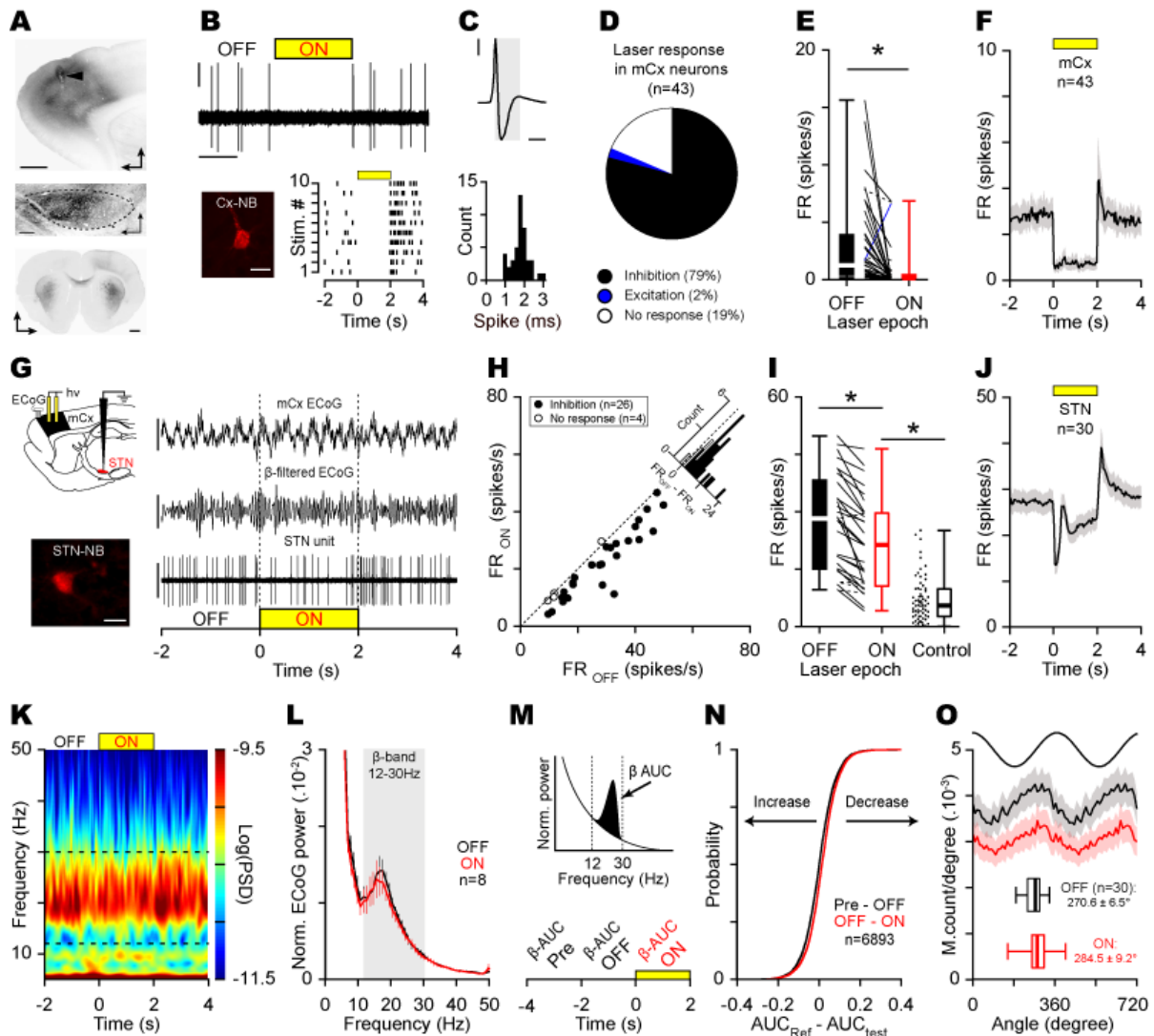


Figure 1. Motor cortex activity is not necessary for abnormal network dynamics in cortico-BG loop. (A) Epifluorescent images showing eArchT3-EYFP labelling in mCx (top, scale: 1 mm), STN (middle, scale: 200 μ m), and striatum (bottom, scale: 1 mm) of 6-OHDA rats. Arrowhead indicates the optic fiber track in mCx. (B) Opto-inhibition example of a pyramidal neuron (top, scales: 0.5 mV, 1 s) labelled juxtacellularly with neurobiotin (bottom left, scale bar: 20 μ m) and corresponding raster plot (bottom right). (C) Example of action potentials waveform average (top, scales: 0.5mV, 1 ms, same neuron as in B) and spike duration distribution for mCx recorded neurons (bottom, bin: 0.2 ms). (D) Proportion of mCx neurons inhibited (black), excited (blue), or not-modulated (white) by laser stimulation. (E) Box-and-whisker plots comparing mCx firing rate during OFF/ON laser epochs; firing rate (FR). (F) Population PSTH in mCx during laser stimulation (bin: 50 ms). (G) Experimental paradigm (top left) and representative example of ECoG (top right, scales: 100 μ V), β -filtered ECoG signal (12-30 Hz, middle right, scale: 50 μ V), and one STN unit (bottom right, scale: 2 mV) during mCx opto-inhibition. Juxtacellular neurobiotin labelling confirmed STN recordings (bottom left, scale: 20 μ m). (H) Scatter plots of STN neurons firing rate during ON vs. OFF laser stimulation. (I) Box-and-whisker plots of STN firing rate during OFF/ON laser epochs in PD rats, and in control animals. (J) Population PSTH of STN firing during mCx opto-inhibition (bin: 50 ms). (K) Peri-event spectrogram of mCx ECoG recording during mCx opto-inhibition. (L) Mean normalized power spectrum of mCx ECoG during OFF vs. ON laser epochs (analysis on the best β epochs for each rat). (M) Schematic of the β -AUCs calculation (top) that we performed at three consecutive time periods: ‘Pre’, ‘OFF’, and ‘ON’ laser stimulation (bottom) for every single opto-stimulation epoch. (N) Cumulative distribution function of the β -AUCs differences calculated between $AUC_{(Pre-OFF)}$ and $AUC_{(OFF-ON)}$ for every ECoG β epochs. (O) Mean phase histograms of STN neurons during β -oscillation for the OFF and ON laser epochs. Group data represents mean \pm SEM, box-and-Whisker plots indicate median, first, third quartile, min and max values. See also Table S1.

Figure 2

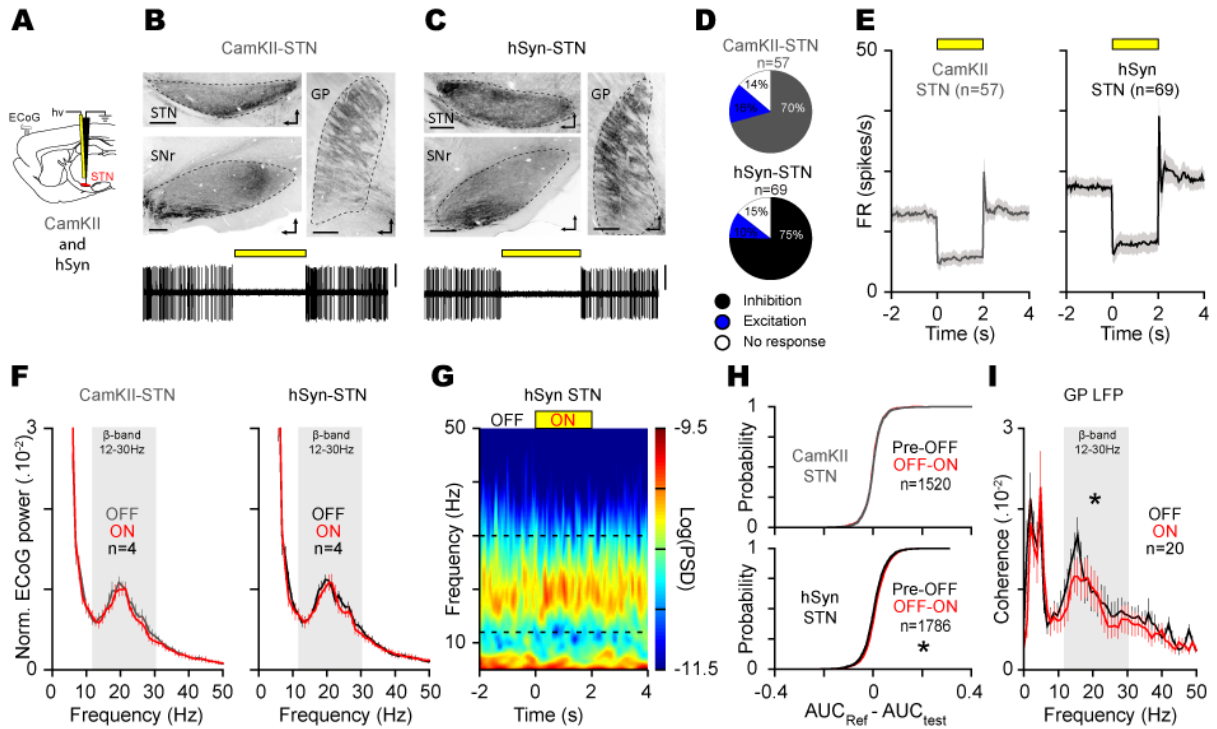


Figure 3

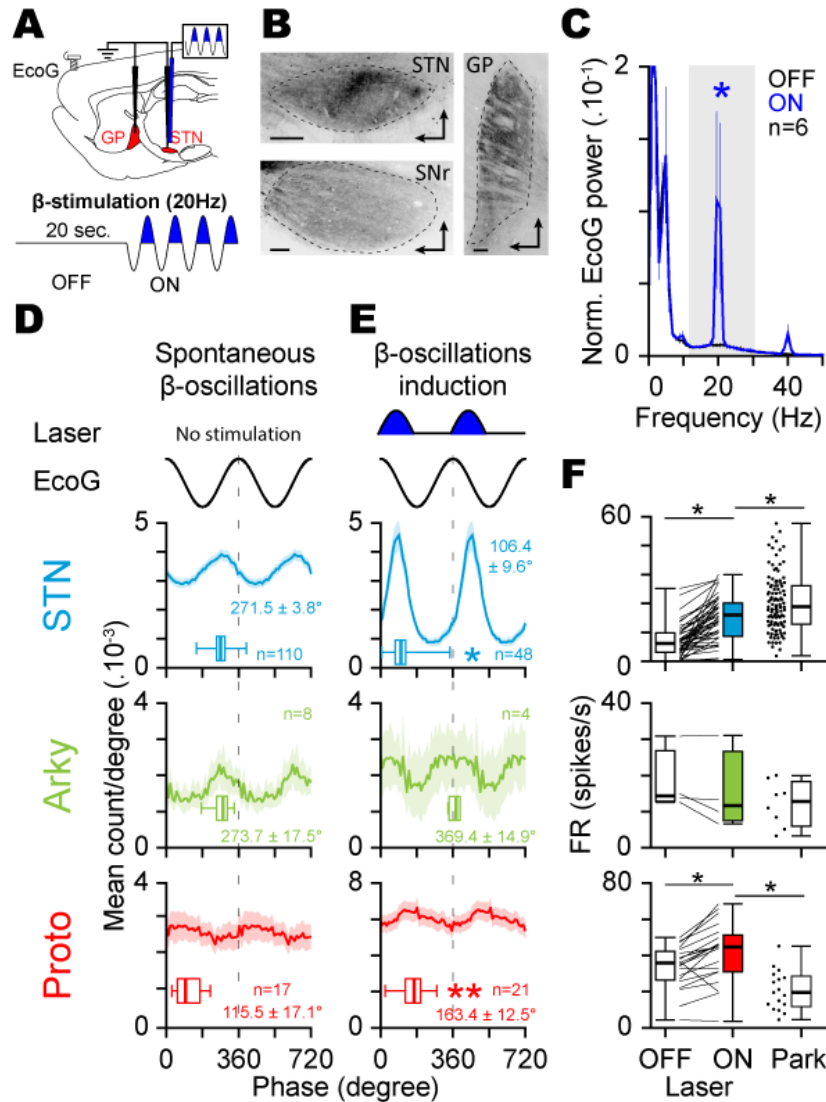


Figure 3. Excitatory optogenetic patterning of STN neurons at β frequency does not replicate the functional properties of parkinsonian β -oscillations. (A) Schematic of the experiment in ChR2-expressing STN neurons (top) and laser stimulation protocol (bottom) used to mimic abnormal β -oscillations in normal rats. (B) Sagittal epifluorescence images showing the ChR2-EYFP labelling at the level of the STN (top left) and their axons in SNr (bottom left) and GP (right) (scale: 200 μ m). Slices orientation: dorso-rostral. (C) Mean power spectrum of mCx EcoG during OFF and ON laser stimulation in normal rat. (D) Mean phase histograms of STN (top), arypallidal (middle), and prototypic (bottom) neurons during abnormal β -oscillations recorded in 6-OHDA-lesioned rats. (E) Mean phase histograms of STN (top), arypallidal (middle), and prototypic (bottom) neurons during synthetic β -oscillations evoked via opto-patterning of STN neurons using ChR2 in control rats. (F) Comparison of the change in firing rate induced by synthetic β as compared to abnormal parkinsonian β in STN, arypallidal, and prototypic neurons. Group data represents mean \pm SEM, box-and-Whisker plots indicate median, first and third quartile, min and max values. See also Table S3.

Figure 4

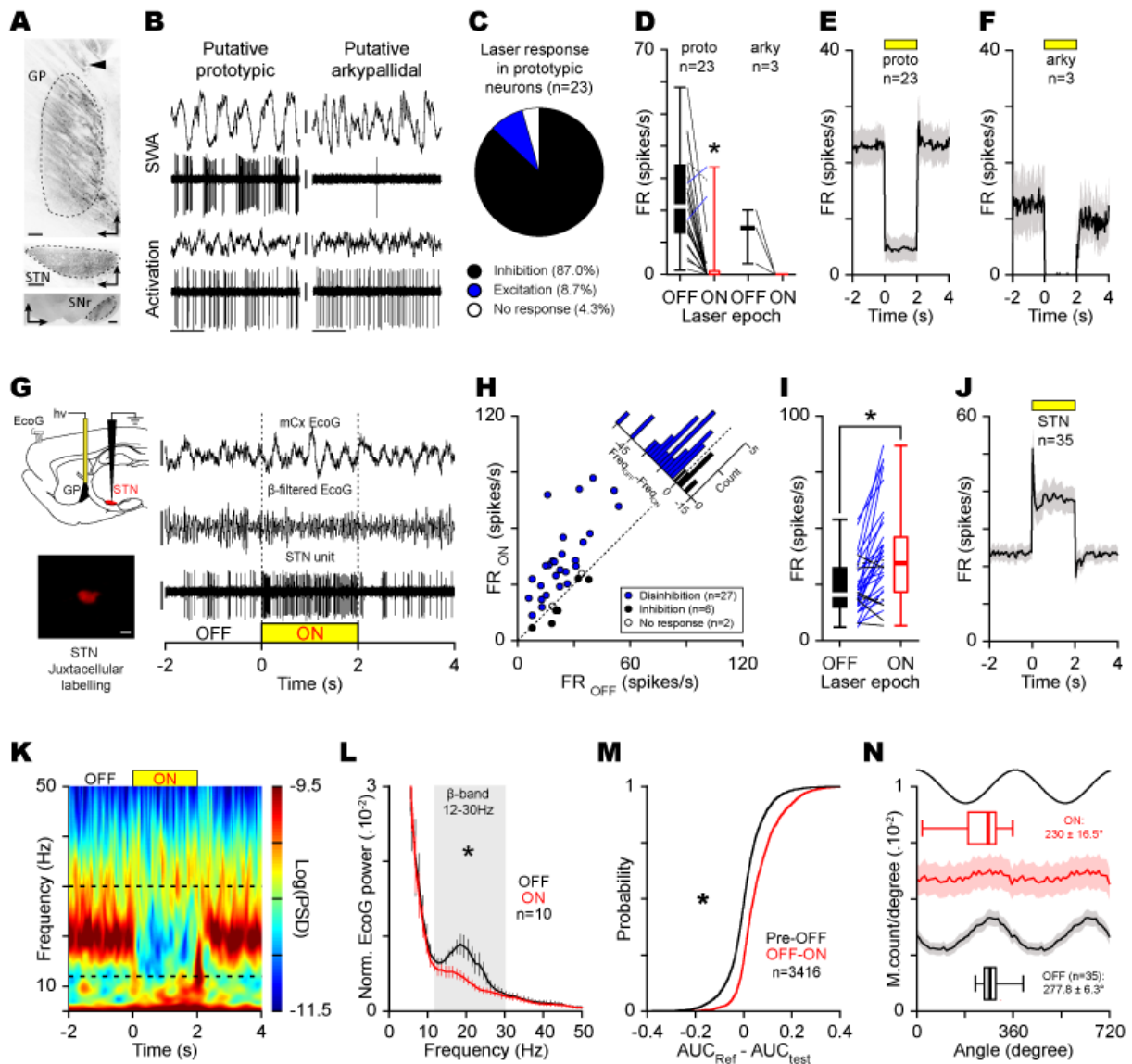


Figure 4. Globus pallidus opto-inhibition suppresses parkinsonian abnormal β -synchronization in cortico-BG loop. (A) Epifluorescence images showing the eArch3-EYFP labelling in GP of 6-OHDA rats (top, scale: 200 μ m, arrowhead indicates the optic fiber track) and axonal labelling in STN (middle, scale: 200 μ m) and SNr (bottom, scale: 500 μ m). (B) Electrophysiological activity of prototypic and arkyallidal neurons during SWA (top) and global activation (bottom). ECoG scale: 0.2 mV; Spike unit: 0.5 mV. (C) Proportion of GP neurons inhibited (black), excited (blue), or not-modulated (white) by laser stimulation. (D) Effect of opto-inhibition on prototypic and arkyallidal firing. (E, F) Population PSTH of opto-inhibition on prototypic (E) and arkyallidal neurons (F) (bin: 50 ms). (G) Experimental paradigm (top left) and representative recordings of ECoG (scales: 250 μ V), β -filtered ECoG (12-30 Hz, scale: 250 μ V) and one STN unit (scale: 1 mV) during GP opto-inhibition. Example of juxtacellularly labelled STN neuron (bottom left, scale: 20 μ m). (H) Scatter plot of GP opto-inhibition on STN firing. (I) STN firing rate changes during OFF vs. ON GP opto-inhibition. (J) Mean PSTH of STN during laser stimulations (bin: 50 ms). (K) Peri-event spectrogram of mCx ECoG illustrating the impact of GP opto-inhibition during β -oscillations. (L) Mean **normalized** power spectrum of mCx ECoG OFF vs. ON GP opto-inhibition (analysis on the best β epochs). (M) Cumulative distribution function of the β -AUCs differences calculated for $AUC_{(Pre-OFF)}$ vs. $AUC_{(OFF-ON)}$ for all ECoG β epochs during GP opto-inhibition. (N) Mean phase histograms of STN neurons during β -oscillations OFF vs. ON laser epochs. Group data represents mean \pm SEM, box-and-Whisker plots indicate median, first and third quartile, min and max values. See also Table S4.

Figure 5

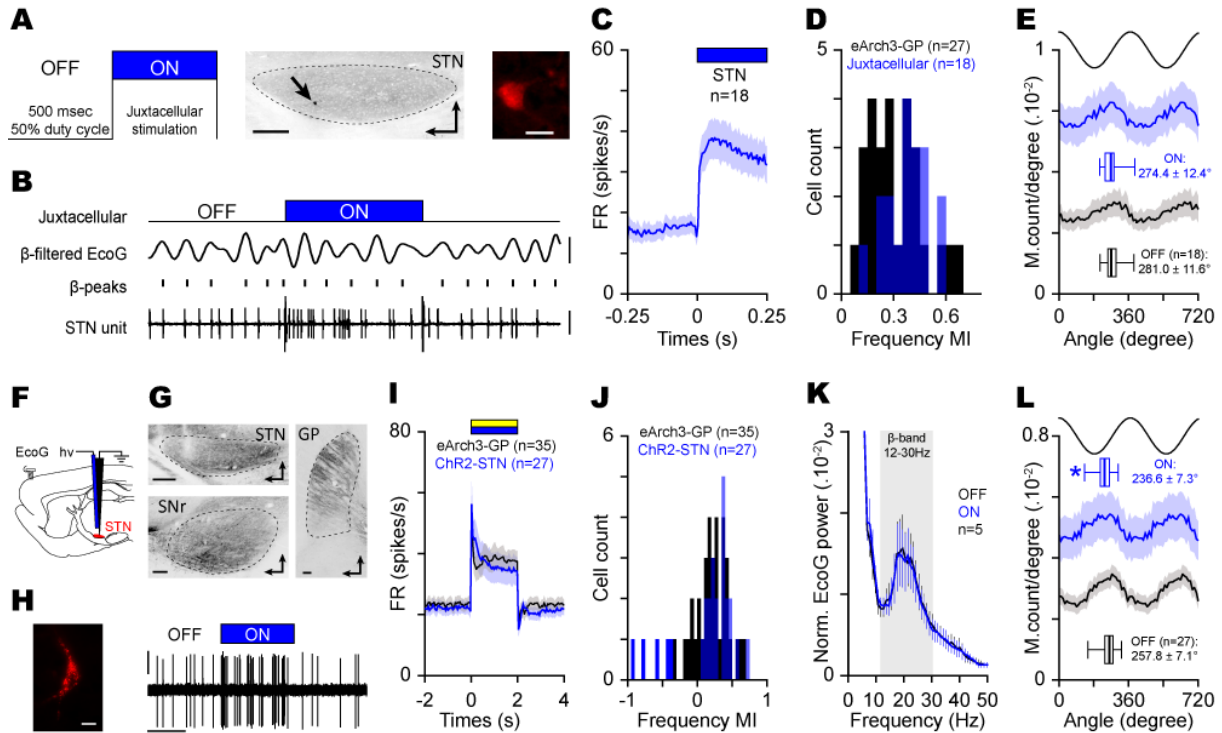


Figure 5. Change in STN firing rate does not suppress abnormal β -synchronization. (A) Juxtacellular stimulation protocol used to increase the firing rate of single STN neuron as revealed by neurobiotin labelling on sagittal STN epifluorescence image (left image: arrow indicate cell body labelled, scale: 200 μ m; right image: neurobiotin-labelled STN neuron, scale 20 μ m). (B) Example of STN neuron firing increase during juxtacellular stimulation (scales bars are β -filtered ECoG: 50 μ V, Spike: 2 mV, Time: 750 ms). (C) Population PSTH of all juxtacellularly-excited STN neurons recorded during β -oscillations epochs (bin: 5 ms). (D) Comparison of the modulatory index (MI) distribution obtained from juxtacellularly-excited STN neurons as compared to disinhibited STN neurons from eArch3-GP opto-inhibition. (E) Mean phase histograms of the juxtacellularly-excited STN neurons during β -oscillation during OFF vs. ON juxtacellular stimulation epochs. (F) Schematic illustration of the electrophysiological recordings in STN expressing ChR2-EYFP in 6-OHDA rats. (G) Sagittal epifluorescence images illustrating the ChR2-EYFP signal at the level of STN (top left) and axon terminals in SNr (bottom left) and GP (right). Scale bar represent 200 μ m. (H) Example of STN opto-excitation during laser stimulation (right, scales bars are: 0.5 mV, 1 s) and labelled with neurobiotin (left, scale bar is 20 μ m). (I) Comparison of population PSTH between all ChR2-excited STN neurons and all STN neurons during eArch3-GP opto-inhibition (bin: 50 ms). (J) Distribution of the MI obtained from ChR2-excited STN neurons and disinhibited STN neurons during eArch3-GP inhibition. (K) Mean **normalized** power spectrum of mCx ECoG during OFF and ON laser epochs (analysis on the best β epochs for each rat). (L) Mean phase histograms of the STN neurons during OFF and ON laser epochs. Group data represents mean \pm SEM, box-and-Whisker plots indicate median, first and third quartile, min and max values. See also Table S5.

Figure 6

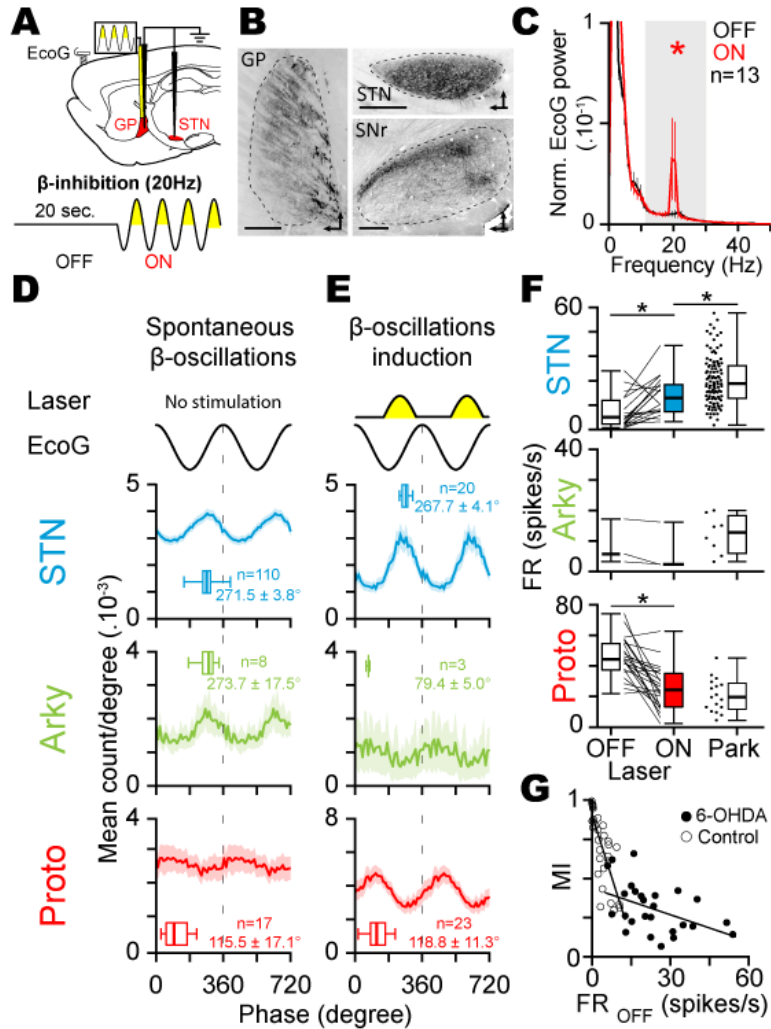


Figure 6. Optogenetic patterning of GP neurons at β frequency replicates the core functional properties of parkinsonian β -oscillations. (A) Schematic of the experiments (top) and laser stimulation protocol used (bottom) to reintroduce abnormal β -oscillations in control rats. (B) Sagittal epifluorescence image of eArch3-EYFP expression in GP (right) and target structures in STN (top left) and SNr (bottom left). Scale bars represent 400 μ m. (C) Mean **normalized** power spectrum of mCx ECoG during OFF and ON laser stimulations. (D, E) Mean phase histograms of STN (top), arky pallidal (middle), and prototypic (bottom) neurons during parkinsonian β -oscillations recorded in PD rats (D) or during synthetic β -oscillations generated via GP neurons opto-patterning using eArch3 in control rats (E). (F) Comparison of the firing rate changes induced by synthetic β as compared to parkinsonian β in STN, arky pallidal, and prototypic neurons. (G) Scatter plots and linear regression of the MI vs. frequency OFF calculated for all STN neurons recorded in control animals (open circle) or parkinsonian rats (black circle). Group data represents mean \pm SEM, box-and-Whisker plots indicate median, first and third quartile, min and max values. See also Table S6.

Supplemental Information:

Table S1. Relates to Figure 1

| Figure | Parameter | n (rats/neurons) | Data Type | Data Value | Statistical test | significance level |
|-----------|------------------------|------------------|-----------|------------------------------|----------------------------|--------------------|
| 1E | Firing Rate | 5 /43 | OFF | 2.8 ± 0.6 | Wilcoxon signed rank test | $z=-5.23, p<0.001$ |
| | | | ON | 0.7 ± 0.3 | | |
| 1I | Firing Rate | 8/30 | OFF | 27.3 ± 2.3 | Wilcoxon signed rank test | $z=-4.70, p<0.001$ |
| | | | ON | 21.7 ± 2.2 | Mann-Whitney Rank Sum Test | |
| | | 15/68 | Control | 7.0 ± 0.7 | | |
| 1L | β -AUC power | 8/8 rec. | OFF | $1.7 \pm 0.1 \times 10^{-1}$ | paired <i>t</i> -test | $t=1.69, p=0.135$ |
| | | | ON | $1.6 \pm 0.2 \times 10^{-1}$ | | |
| 1N | β -AUC power | 8/6893 opto stim | Pre-OFF | $1.1 \pm 0.8 \times 10^{-3}$ | Wilcoxon signed rank test | $z=-1.53, p=0.126$ |
| | | | OFF-ON | $3.0 \pm 0.8 \times 10^{-3}$ | | |
| 1O | β -phase locking | 8/30 | OFF | $270.6 \pm 6.5^\circ$ | Watson-Williams F test | $F=1.42, p=0.240$ |
| | | | ON | $284.5 \pm 9.2^\circ$ | | |

Table S2. Relates to Figure 2

| Figure | Parameter | n (rats/neurons) | Data Type | Data Value | Statistical test | significance level |
|-------------------------------|------------------------|------------------|-----------|-------------------------------|---------------------------|--------------------|
| 2E, CaMKII α | Firing Rate | 4/57 | OFF | 16.0 ± 1.4 | Wilcoxon signed rank test | $z=-4.46, p<0.001$ |
| | | | ON | 6.9 ± 1.3 | | |
| 2E, hSyn | Firing Rate | 4/69 | OFF | 21.7 ± 1.7 | paired <i>t</i> -test | $t=5.17, p<0.001$ |
| | | | ON | 9.9 ± 1.9 | | |
| 2F, CaMKII α | β -AUC power | 4/4 rec. | OFF | $1.5 \pm 0.3 \times 10^{-1}$ | —* | —* |
| | | | ON | $1.2 \pm 0.2 \times 10^{-1}$ | | |
| 2F, hSyn | β -AUC power | 4/4 rec. | OFF | $1.5 \pm 0.03 \times 10^{-1}$ | —* | —* |
| | | | ON | $1.5 \pm 0.07 \times 10^{-1}$ | | |
| 2H, CaMKII α | β -AUC power | 4/1520 opto stim | Pre-OFF | $1.9 \pm 1.0 \times 10^{-3}$ | Wilcoxon signed rank test | $z=1.11, p=0.265$ |
| | | | OFF-ON | $-7.5 \pm 1.0 \times 10^{-3}$ | | |
| 2H, hSyn | β -AUC power | 4/1786 opto stim | Pre-OFF | $-8.8 \pm 2.6 \times 10^{-3}$ | Wilcoxon signed rank test | $z=-3.63, p<0.001$ |
| | | | OFF-ON | $4.4 \pm 1.9 \times 10^{-3}$ | | |
| 2I | β -AUC coherence | 4/20 rec. | OFF | 1.9 ± 0.4 | paired <i>t</i> -test | $t=4.25, p<0.001$ |
| | | | ON | 1.6 ± 0.4 | | |

* : Sample size too small for statistical analysis.

Table S3. Relates to Figure 3

| Figure | Parameter | n (rats/neurons) | | Data Type | Data Value | Statistical test | significance level |
|-----------|------------------------|------------------|--------|-----------|------------------------------|---------------------------|---------------------|
| 3C | β -AUC power | 6/6 rec. | | OFF | $1.8 \pm 0.2 \times 10^{-4}$ | Wilcoxon signed rank test | $z=2.20, p=0.031$ |
| | | | | ON | $4.6 \pm 0.1 \times 10^{-4}$ | | |
| 3D vs. 3E | β -phase locking | STN | 28/110 | Park | $271.5 \pm 3.8^\circ$ | Watson-Williams F test | $F=339.15, p<0.001$ |
| | | | 6/48 | ON-ChR2 | $106.4 \pm 9.6^\circ$ | | |
| | | Arky | 6/8 | Park | $273.7 \pm 17.5^\circ$ | —* | —* |
| | | | 3/4 | ON-ChR2 | $369.4 \pm 14.9^\circ$ | | |
| | | Proto | 6/17 | Park | $115.5 \pm 17.1^\circ$ | Watson-Williams F test | $F=8.97, p=0.0049$ |
| | | | 5/21 | ON-ChR2 | $163.4 \pm 12.5^\circ$ | | |
| 3F | Firing Rate | STN | 6 /48 | OFF-ChR2 | 7.0 ± 0.8 | Wilcoxon signed rank test | $z=5.990, p<0.001$ |
| | | | | ON-ChR2 | 15.0 ± 1.1 | | |
| | | | 28/110 | Park | 24.3 ± 1.1 | Mann-Whitney | $U=1395, p<0.001$ |
| | | Arky | 3/4 | OFF-ChR2 | 18.0 ± 4.3 | —* | —* |
| | | | | ON-ChR2 | 15.3 ± 5.4 | | |
| | | | 6/8 | Park | 12.2 ± 2.2 | —* | —* |
| | | Proto | 5/21 | OFF-ChR2 | 33.7 ± 2.6 | paired <i>t</i> -test | $t=4.48, p=0.032$ |
| | | | | ON-ChR2 | 41.7 ± 3.6 | | |
| | | | 6/17 | Park | 20.8 ± 2.6 | <i>t</i> -test | $t=-4.52, p<0.001$ |

* : Sample size too small for statistical analysis.

Table S4. Relates to Figure 4

| Figure | Parameter | n (rats/neurons) | | Data Type | Data Value | Statistical test | significance level |
|--------|--------------------|---------------------|------|-----------------------------|-----------------------------|---------------------------|----------------------------|
| 4D | Firing Rate | Proto | 5/23 | OFF | 22.9 ± 3.0 | paired <i>t</i> -test | t=5.69, <i>p</i> <0.01 |
| | | | | ON | 4.7 ± 2.1 | | |
| | | Arky | 5/3 | OFF | 12.6 ± 4.9 | —* | —* |
| | | | | ON | 0.03 ± 0.03 | | |
| 4I | Firing Rate STN | 10/35 | | OFF | 23.8 ± 2.0 | Wilcoxon signed rank test | z=4.472, <i>p</i> <0.001 |
| | | | ON | 38.6 ± 3.5 | | | |
| 4L | β -AUC power | 10/10 | | OFF | 1.2 ± 0.5 x10 ⁻¹ | paired <i>t</i> -test | t=4.188, <i>p</i> =0.002 |
| | | | ON | 0.8 ± 0.3 x10 ⁻¹ | | | |
| 4M | β -AUC power | 10/3416 opto stim | | Pre-OFF | 2.7 ± 1.1 x10 ⁻³ | Wilcoxon signed rank test | z=-27.025, <i>p</i> <0.001 |
| | | | | OFF-ON | 5.6 ± 2.3 x10 ⁻³ | | |

* : Sample size too small for statistical analysis.

Table S5. Relates to Figure 5

| Figure | Parameter | n (rats/neurons) | | Data Type | Data Value | Statistical test | significance level |
|--------|------------------------|---------------------|-------------|-----------------------------|-----------------------------|--------------------------------|---------------------------------|
| 5C | Firing Rate | 9/18 | | OFF-Juxta | 23.5 ± 2.7 | paired <i>t</i> -test | t=-7.62, <i>p</i> <0.001 |
| | | | | ON-Juxta | 52.2 ± 5.6 | | |
| 5D | MI | 10/27 | MI Arch3-GP | 3.0 ± 0.3 x10 ⁻¹ | <i>t</i> -test | t=-1.65, <i>p</i> =0.107 | |
| | | 9/18 | MI juxta | 3.8 ± 0.3 x10 ⁻¹ | | | |
| 5E | β -phase locking | 9/18 | | OFF-Juxta | 281.0 ± 11.6° | Watson-Williams F test | ns (F=0.29, <i>p</i> =0.593) |
| | | | | ON-Juxta | 274.4 ± 12.4 ° | | |
| 5I | Firing Rate | 5/27 | | OFF | 22.2 ± 2.0 | paired <i>t</i> -test | t=-3.96, <i>p</i> <0.001 |
| | | | | ON | 37.3 ± 5.2 | | |
| 5J | MI | 10/35 | MI Arch3-GP | 2.1 ± 0.4 x10 ⁻¹ | Mann-Whitney rank sum test | ns (U=457, <i>p</i> =0.831) | |
| | | 5/27 | MI Chr2-STN | 1.2 ± 0.8 x10 ⁻¹ | | | |
| 5K | β -AUC power | 5/5 | | β -AUC OFF | 2.2 ± 0.4 x10 ⁻¹ | paired <i>t</i> -test | ns (t=0.919, <i>p</i> =0.41) |
| | | | | β -AUC ON | 2.1 ± 0.4 x10 ⁻¹ | | |
| 5L | β -phase locking | 5/27 | | OFF | 257.8 ± 7.1 ° | Watson-Williams F test | F=4.90 <i>p</i> =0.0313 |
| | | | | ON | 236.6 ± 7.3 ° | | |

Table S6. Relates to Figure 6

| Figure | Parameter | n (rats/neurons) | | Data Type | Data Value | Statistical test | significance level |
|------------------|------------------------|------------------|--------|-----------|------------------------------|---------------------------|------------------------------|
| 6C | β -AUC power | 13/13 rec. | | OFF | $1.2 \pm 0.2 \times 10^{-1}$ | Wilcoxon signed rank test | $Z=2.970, p=0.001$ |
| | | | | ON | $1.9 \pm 0.7 \times 10^{-1}$ | | |
| 6D vs. 6E | β -phase locking | STN | 28/110 | Park | $271.5 \pm 3.8^\circ$ | Watson-Williams F test | ns ($F=0.763, p=0.50$) |
| | | | 13/20 | ON | $267.7 \pm 4.1^\circ$ | | |
| | | Arky | 6/8 | Park | $273.7 \pm 17.5^\circ$ | —* | —* |
| | | | 13/3 | ON | $79.4 \pm 5.0^\circ$ | | |
| | | Proto | 6/17 | Park | $115.5 \pm 17.1^\circ$ | Watson-Williams F test | ns ($F=0.830, p=0.367$) |
| | | | 13/23 | ON | $118.8 \pm 11.3^\circ$ | | |
| 6F | Firing Rate | STN | 13/20 | OFF | 7.1 ± 1.5 | paired <i>t</i> -test | $t=-3.50, p=0.002$ |
| | | | | ON | 13.6 ± 1.8 | | |
| | | | 28/110 | Park | 24.3 ± 1.1 | Mann-Whitney | $U=486, p<0.001$ |
| | | Arky | 3/3 | OFF | 8.8 ± 4.3 | —* | —* |
| | | | | ON | 7.0 ± 4.6 | | |
| | | | 6/8 | Park | 12.2 ± 2.2 | —* | —* |
| | | Proto | 13/23 | OFF | 45.5 ± 2.7 | paired <i>t</i> -test | $t=5.30, p<0.001$ |
| | | | | ON | 25.9 ± 3.0 | | |
| | | | 6/17 | Park | 20.8 ± 2.6 | Mann-Whitney | ns ($U=151, p=0.229$) |
| | | 6G | MI | 18/32 | | control | $y = 0.92 - 0.05x$ |
| 10/27 | | | | Park | $y = 0.44 - 0.006x$ | Linear regression | $p=0.012, r^2=0.23$ |

* : Sample size too small for statistical analysis.

Figure S1

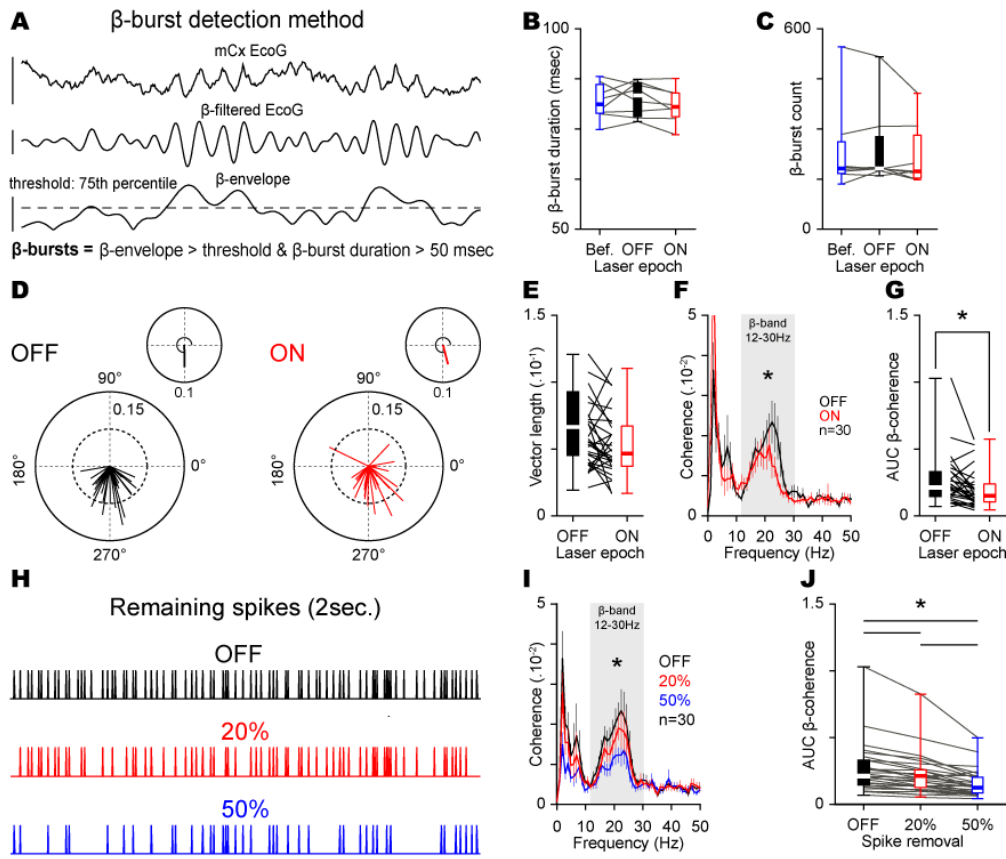


Figure S1. Effect of mCx opto-inhibition on abnormal network dynamics in Parkinsonism. (A) Analytical approach used to detect the bursts of β oscillations. Representative example of ECoG (scales: 200 μ V), β -filtered signal (12-30 Hz, scale: 50 μ V), and β -envelopes (scale: 0.04 unit) with the 75th percentile threshold (dashed line). (B-C) Box-and-whisker plots showing the effect of mCx opto-inhibition on the β -bursts duration (B, Before in blue vs. OFF in black vs. ON in red, $n=8$, β -bursts duration Before vs. OFF vs. ON, $8.33 \pm 0.17 \times 10^{-2}$ vs. $8.43 \pm 0.16 \times 10^{-2}$ vs. $8.24 \pm 0.16 \times 10^{-2}$ s, One Way Repeated Measures Analysis of Variance, $F=1.19$, $p=0.33$) and β -burst counts (C, $n=8$, β -bursts counts Before vs. OFF vs. ON, 231.9 ± 47.37 vs. 235.9 ± 43.25 vs. 215.6 ± 32.92 β -bursts, Friedman Repeated Measures Analysis of Variance on Ranks, $X^2=0.84$, $p=0.65$). (D) Individual and mean circular phase of phase-locked STN neurons during OFF and ON laser stimulation epochs ($n=30$, OFF vs. ON, $270.6 \pm 6.5^\circ$ vs. $284.5 \pm 9.2^\circ$, Watson-Williams F test, $F=1.42$, $p=0.240$). (E) Box-and-whisker plots showing the change in vector lengths induced by mCx opto-inhibition ($n=30$, OFF vs. ON, $5.9 \pm 0.4 \times 10^{-2}$ vs. $5.3 \pm 0.4 \times 10^{-2}$, paired t -test, $t=1.70$, $p=0.101$). (F-G) Mean coherence (F) and box-and-whisker plots of the β -band coherence (G) between mCx ECoG and STN unit during OFF and ON laser stimulation epochs ($n=30$, AUC β -band coherence OFF vs. ON, $2.6 \pm 0.3 \times 10^{-1}$ vs. $2.0 \pm 0.3 \times 10^{-1}$, Wilcoxon signed rank test, $z=-2.71$, $p=0.007$). (H) Example of random spike removal reaching 20% (red), or 50% (blue) of the reference OFF stimulation epoch in one STN neuron (black). (I-J) Mean coherence (I) and box-and-whisker plots of the β -band coherence (J) between mCx ECoG and STN unit without (OFF, black) or with random spike removal (20% in red, 50% in blue, $n=30$, AUC β -band OFF vs. OFF 80% vs. OFF 50% vs. ON, $2.6 \pm 0.3 \times 10^{-1}$ vs. $2.1 \pm 0.3 \times 10^{-1}$ vs. $1.6 \pm 0.2 \times 10^{-1}$ vs. $2.0 \pm 0.3 \times 10^{-1}$, Friedman repeated measures ANOVA on ranks, $X^2=50.04$, $p<0.001$, following by Dunn's post hoc test, $p<0.05$ for OFF vs. OFF 80%, OFF vs. OFF 50%, OFF vs. ON and OFF 80% vs. OFF 50%, $q=3.9$, 6.9, 4.8 and 3.0 respectively).

Figure S2

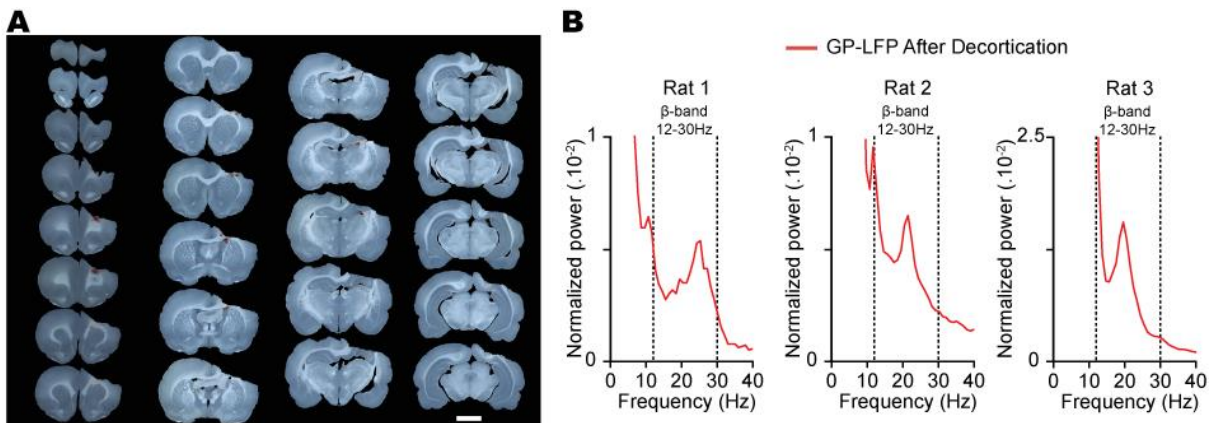


Figure S2. Decortication experiments in 6-OHDA lesioned rats. (A) Bright-field images of coronal brain sections organized in a serial manner from rostral to caudal sections and illustrating the extend of the decortication. (B) Power spectra illustrating the peak in the β frequency band (12-30 Hz) present in GP local field potentials (LFPs) recorded in 3 different 6-OHDA-lesioned rats after decortication. Although the exact generation mechanism of LFPs in non-layered structure such as basal ganglia is unclear, GP-LFPs were used here as a proxy of neuronal synchronization as previously shown during β -oscillations²⁶.

Figure S3

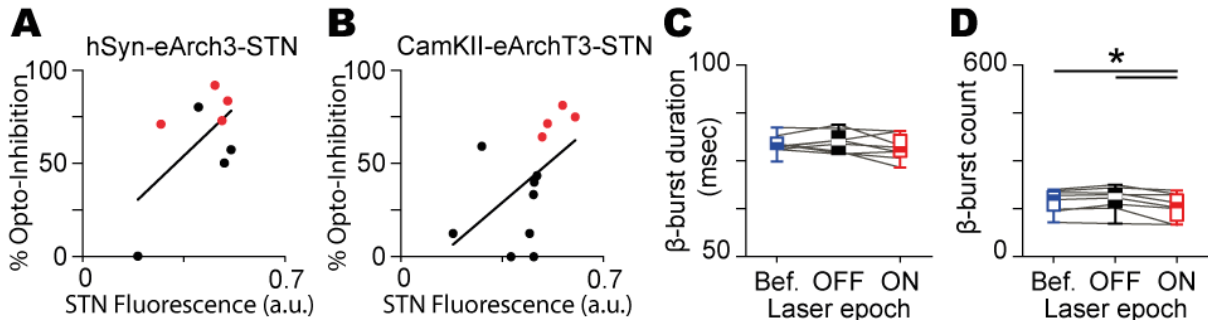


Figure S3. Quantification of STN opto-inhibition and effect on β bursts dynamics. (A- B) Correlation analysis between the percentage of STN opto-inhibition determined through opto-mapping experiments and the mean EYFP fluorescence in STN for hSyn-eArch3 (A, linear regression $r^2 = 0.3741$) or CamKII-eArchT3 (B, linear regression $r^2 = 0.2664$) experiments. Red and black dots indicate the animals included or excluded from the study, respectively. Animals were discarded if they had less than 10 STN neurons recorded during opto-mapping or if the total % of STN opto-inhibition was < to 60%. (C-D) Box-and-whisker plots showing the effect of STN opto-inhibition on the β -bursts duration (C, $n=8$, β -burst duration Before vs. OFF vs. ON, $7.96 \pm 0.07 \times 10^{-2}$ vs. $7.99 \pm 0.1 \times 10^{-2}$ vs. $7.83 \pm 0.1 \times 10^{-2}$ s, One Way Repeated Measures Analysis of Variance, $F=1.81$, $p=0.20$) and β -bursts counts ($n=8$, β -burst duration Before vs. OFF vs. ON, 172.75 ± 13.0 vs. 179.63 ± 13.9 vs. 157.88 ± 14.8 β -bursts, Friedman Repeated Measures Analysis of Variance on Ranks, $F=7.19$, $p=0.007$, following by Holm-Sidak post hoc test, OFF vs. Before, OFF vs. ON and Before vs. ON, $t=1.17$, 3.71 and 2.54 , $p=0.26$, 0.007 and 0.047 , respectively).

Figure S4

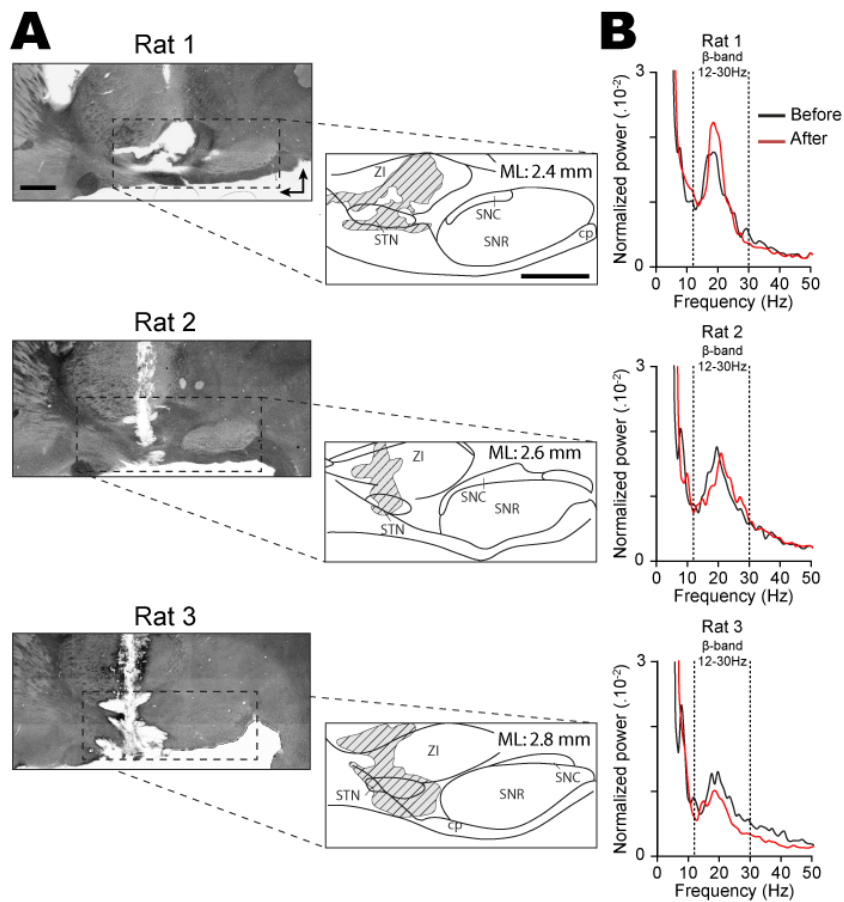


Figure S4. Effect of STN lesion on β -oscillations expression in 6-OHDA lesioned rats. (A) Epifluorescent images showing DAPI staining (left) and schematic representation (right) of sagittal rat brain sections illustrating the extent of the STN electrolytic lesion (hashed grey area). Scale bar represent 1 mm. **(B)** Power spectrums illustrating the peak in the β frequency band (12-30 Hz) present in the ECoG before and after the full lesion of the STN in 3 different 6-OHDA-lesioned rats.

Figure S5

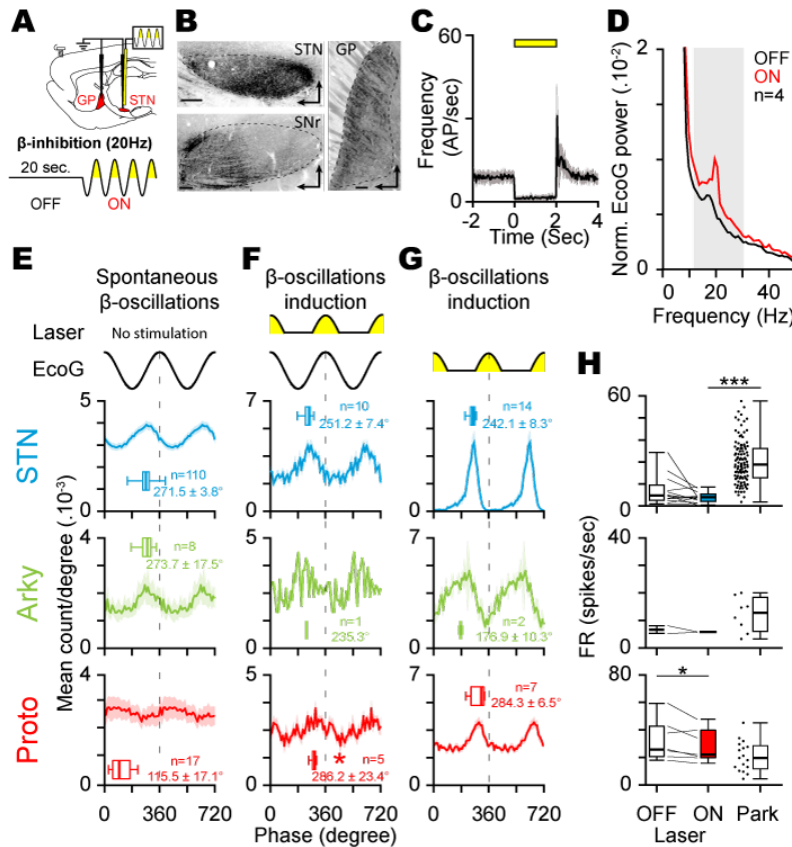


Figure S5. Inhibitory optogenetic patterning of STN neurons at β frequency does not replicate the functional properties of parkinsonian β -oscillations. (A) Schematic of the experiment in eArchT3.0-expressing STN neurons (top) and laser stimulation protocol (bottom) used to mimic abnormal β -oscillations in normal rats. (B) Sagittal epifluorescence images showing the eArchT3.0-EYFP labelling at the level of the STN (top left) and their axons in SNr (bottom left) and GP (right) (scale: 200 μ m). Slices orientation: dorso-rostral. (C) Mean PSTH of STN neurons during laser stimulations (bin: 50 ms, STN-OFF vs. STN-ON, n=16, 8.90 ± 2.03 vs. 1.37 ± 0.91 spikes/s, Wilcoxon signed rank test, $z=-2.95$, $p=0.002$). (D) Mean normalized power spectrum of mCx ECoG during OFF and ON laser stimulation in normal rat. (E) Mean phase histograms of STN (top), arky (middle), and prototypic (bottom) neurons during abnormal β oscillations recorded in 6-OHDA-lesioned rats. (F) Mean phase histograms of STN (top), arky (middle), and prototypic (bottom) neurons calculated from the cortical β oscillations signal evoked by our opto-patterned stimulation. The mean phase value of STN neurons is not statistically different in the parkinsonian vs. the eArchT3.0 condition (STN-Park vs. STN-ON, n=110 vs. 10, $271.5 \pm 3.8^\circ$ vs. $251.2 \pm 7.4^\circ$, Watson-Williams test, $F=2.52$, $p=0.1153$), whereas the mean phase for prototypic neurons is different (Proto-Park vs. Proto-ON, n=17 vs. 5, $115.5 \pm 17.1^\circ$ vs. $286.2 \pm 23.4^\circ$, Watson-Williams test, $F=17.74$, $p=0.0004$). (G) Mean phase histograms of STN (top), arky (middle), and prototypic (bottom) neurons directly calculated from the peak of the laser stimulation sine waves. These phase histograms better illustrate the phase relationships between STN and GP neurons during β cycles. (H) Comparison of the change in firing rate induced by synthetic β as compared to abnormal parkinsonian β -oscillations in STN (STN-OFF vs. STN-ON, n=13, 8.5 ± 2.2 vs. 4.9 ± 0.8 spikes/sec, Wilcoxon signed rank test, $Z=-1.642$, $p=0.110$; STN-Park vs. STN-ON, n=110 vs. 13, 24.3 ± 1.1 vs. 4.9 ± 0.8 spikes/sec, Mann-Whitney rank sum test, $U=160.0$, $p<0.001$), arky (Arky-OFF vs. Arky-ON, n=2, 6.7 ± 1.4 vs. 5.8 ± 0.1 spikes/sec; Arky-Park vs. Arky-ON, n=8 vs. 2, 12.2 ± 2.2 vs. 5.8 ± 0.1 spikes/sec), and prototypic neurons (Proto-OFF vs. Proto-ON, n=7, 32.8 ± 5.6 vs. 28.7 ± 4.5 spikes/sec, paired t-test, $t=2.321$, $p=0.059$; Proto-Park vs. Proto-ON, n=17 vs. 7, 20.8 ± 2.7 vs. 28.7 ± 4.5 spikes/sec, t-test, $t=2.211$, $p=0.038$). Group data represents mean \pm SEM, box-and-Whisker plots indicate median, first and third quartile, min and max values.

Figure S6

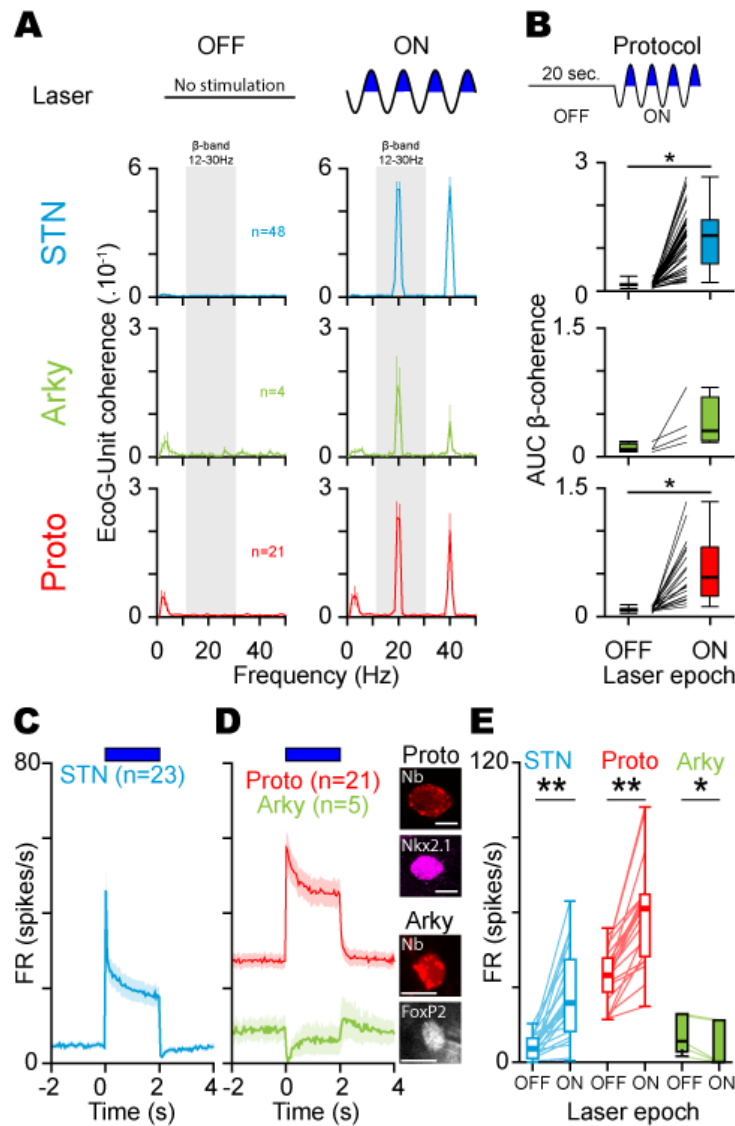


Figure S6. Optogenetic patterning of Chr2-expressing STN neurons at β frequency. (A) Mean Coherence calculated during the OFF vs. ON laser stimulation between mCx ECoG and STN (blue, $n=48$, AUC β -coherence OFF vs. ON: 0.1 ± 0.007 vs. 1.2 ± 0.09 , paired t -test, $t=-11.90$, $* p<0.001$), arkyallidal (black, $n=4$, AUC β -coherence OFF vs. ON: 1.0 ± 0.3 vs. $4.0 \pm 1.4 \times 10^{-1}$), and prototypic neurons (red, $n=21$, AUC β -coherence OFF vs. ON: 0.8 ± 0.06 vs. $5.5 \pm 0.8 \times 10^{-1}$, paired t -test, $t=-6.16$). (B) Comparison of the β -coherence (12-30 Hz) OFF vs. ON laser stimulation (box-and-whisker plot, paired t -tests, $* p<0.001$). (C) Population PSTH of Chr2-excited STN neurons in response to a 2 s laser stimulation ($n=23$, firing rate OFF vs. ON, 5.9 ± 0.9 vs. 26.2 ± 3.6 spikes/s, paired t -test, $t=-6.11$, $p<0.001$). (D) Population PSTH of prototypic (red, $n=21$, firing rate OFF vs. ON, 34.2 ± 2.2 vs. 59.4 ± 4.4 spikes/s, paired t -test, $t=-7.85$, $p<0.001$) and arkyallidal neurons (black, $n=5$, firing rate OFF vs. ON, 11.0 ± 3.4 vs. 6.8 ± 4.1 spikes/s, paired t -test, $t=3.44$, $p=0.0260$) in response to STN opto-excitation. Confocal fluorescence images of juxtacellularly-labelled with neurobiotin (Nb; red) and identified GP prototypic Nkx2.1+ (magenta, top) and arkyallidal FoxP2+ neurons (grey, bottom). Scale bars: 10 μ m. (E) Box-and-whisker plots comparing the firing rate during OFF vs. ON STN opto-excitation stimulation (paired t -tests, $* p=0.026$ and $** p<0.001$).

Figure S7

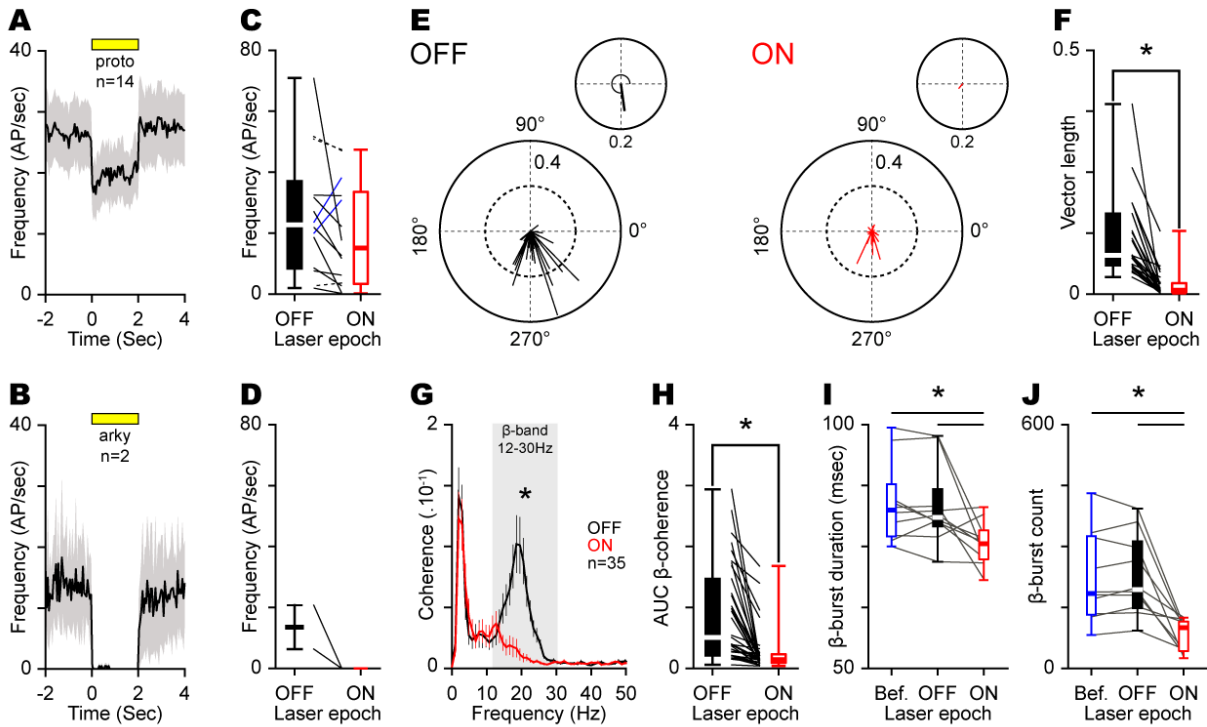


Figure S7. Effect of GP opto-inhibition on abnormal β -oscillations dynamics in Parkinsonism. (A-B) Population PSTH of prototypic ($n=13$, firing rate OFF vs. ON, 26.4 ± 5.4 vs. 19.5 ± 4.5 spikes/s, Wilcoxon signed rank test, $z=-2.93$, $p=0.068$) and arky pallidal neurons ($n=2$, firing rate OFF vs. ON, 13.6 ± 7.2 vs. 0.08 ± 0.08 spikes/s) in response to light stimulation with optic fiber placed 2 mm above the recording electrode (data represent mean \pm SEM, bin: 50 ms). All these neurons were also inhibited with the laser source placed 1 mm (see figure 4). (C-D) Box-and-whisker plots of prototypic (Wilcoxon signed rank test, $*p>0.05$) and arky pallidal neurons during the OFF and ON laser stimulation. (E) Individual and mean circular phase of STN neurons entrained at β frequency during OFF and ON laser stimulation epochs ($n=35$, OFF vs. ON, $277.8 \pm 6.3^\circ$ vs. $230.0 \pm 16.5^\circ$, Watson-Williams F test, $F=0.510$, $p=0.478$). (F) Box-and-whisker plots showing the change in vector lengths induced in STN neurons by GP opto-inhibition ($n=35$, OFF vs. ON, $1.2 \pm 0.1 \times 10^{-1}$ vs. $0.3 \pm 0.06 \times 10^{-1}$, Wilcoxon signed rank test, $z=-5.16$, $p<0.001$). (G-H) Mean coherence (G) and box-and-whisker plots of the β -band (12-30 Hz) coherence (H) between mCx ECoG and STN unit during OFF and ON laser stimulation epochs ($n=35$, AUC β -coherence OFF vs. ON, $8.8 \pm 1.3 \times 10^{-1}$ vs. $2.7 \pm 0.6 \times 10^{-1}$, Wilcoxon signed rank test, $z = -5.086$, $p<0.001$). (I-J) Box-and-whisker plots showing the effect of GP opto-inhibition on the β bursts duration (I, $n=10$, β -burst duration Before vs. OFF vs. ON, $8.39 \pm 0.26 \times 10^{-2}$ vs. $8.31 \pm 0.26 \times 10^{-2}$ vs. $7.56 \pm 0.14 \times 10^{-2}$ s, One Way Repeated Measures Analysis of Variance, $F=6.67$, $p=0.007$, following by Holm-Sidak post hoc test, OFF vs. Before, OFF vs. ON and Before vs. ON, $t=0.28$, 3.01 and 3.30 , $p=0.78$, 0.015 and 0.012 , respectively) and β bursts counts (J, $n=10$, β -burst duration Before vs. OFF vs. ON, 221.5 ± 34.78 vs. 226.70 ± 31.28 vs. 81.80 ± 12.41 β -bursts, Friedman Repeated Measures Analysis of Variance on Ranks, $X^2=15.80$, $p<0.001$, following by Dunn's post hoc test, OFF vs. Before, OFF vs. ON and Before vs. ON, $q=0.89$, 3.80 and 2.91 , $p>0.05$, $p<0.05$ and $p<0.05$ respectively).

Figure S8

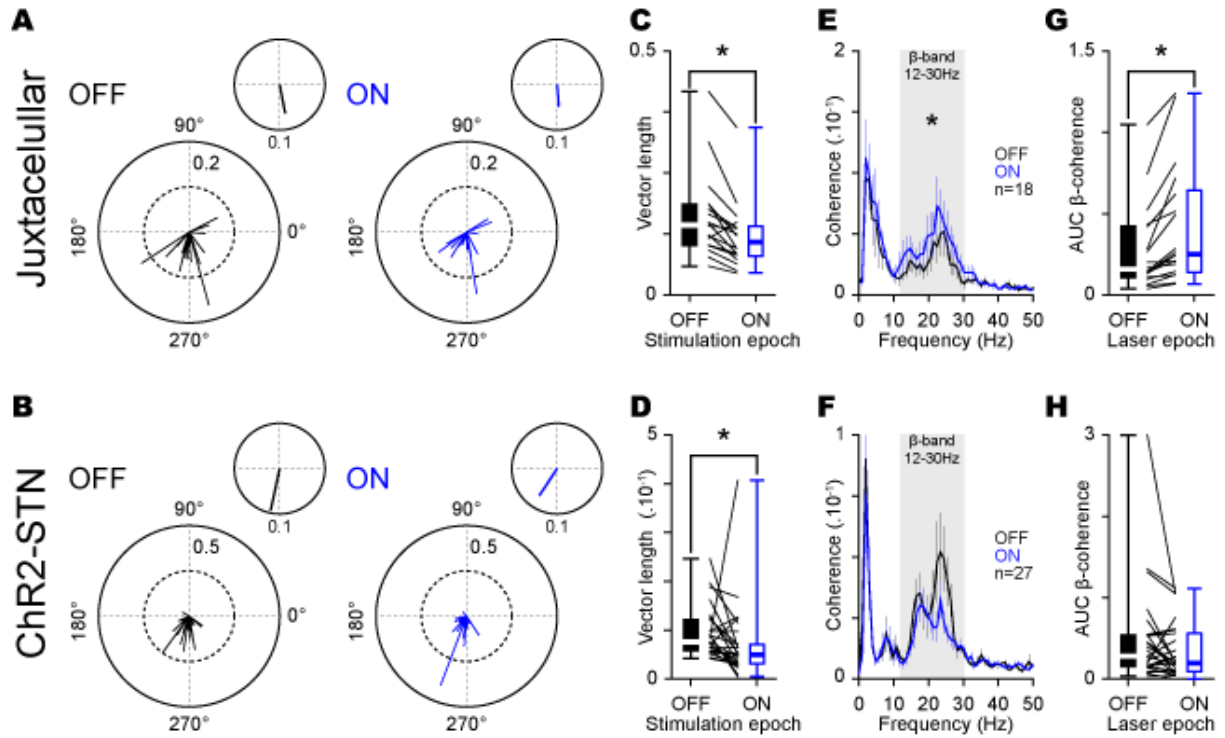


Figure S8. Effect of STN excitation on β -synchronization. (A, B) Individual and mean circular phase of STN neurons entrained at β frequency during OFF vs. ON juxtacellular stimulation epochs (A) or the OFF vs. ON ChR2-STN opto-excitation (B). (C, D) Box-and-whisker plots showing the change in vector lengths induced in STN neurons by the juxtacellular excitation (C, $n=18$, mean vector length OFF-juxta vs. ON-Juxta, $6.4 \pm 0.8 \times 10^{-2}$ vs. $4.9 \pm 0.6 \times 10^{-2}$, paired t -test, $t=4.74$, $p<0.001$) or the ChR2 opto-excitation (D, $n=27$, mean vector length OFF-ChR2 vs. ON-ChR2, $9.5 \pm 1.0 \times 10^{-2}$ vs. $7.1 \pm 1.5 \times 10^{-2}$, Wilcoxon signed rank test, $z=-3.123$, $p=0.002$). (E, F) Mean coherence between mCx ECoG and STN units during OFF vs. ON juxtacellular stimulation (E) or the OFF vs. ON ChR2-STN opto-excitation (F). (G, H) Box-and-whisker plots comparing the β -band (12-30 Hz) coherence during the OFF vs. ON juxtacellular stimulation (G, $n=18$ neurons, AUC β -band coherence OFF-juxta vs. ON-juxta, $2.7 \pm 0.6 \times 10^{-1}$ vs. $4.0 \pm 0.8 \times 10^{-1}$, Wilcoxon signed rank test, $z=3.724$, $p<0.001$) and the OFF vs. ON ChR2-STN opto-excitation (H, $n=27$, AUC β -band coherence OFF-ChR2 vs. ON-ChR2, $5.1 \pm 1.1 \times 10^{-1}$ vs. $3.7 \pm 0.6 \times 10^{-1}$, Wilcoxon signed rank test, $z=-1.802$, $p=0.073$).

Figure S9

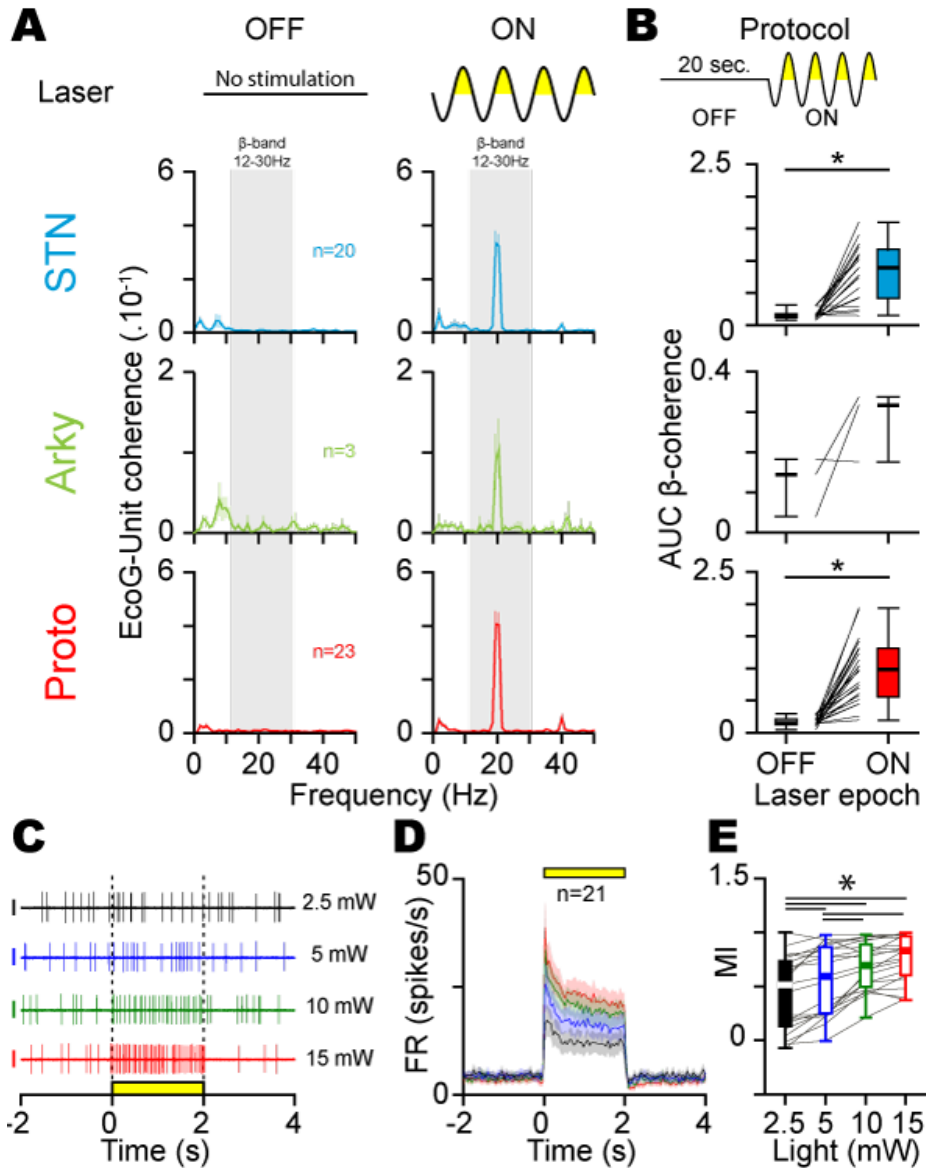


Figure S9. Optogenetic patterning of eArch3-expressing GP neurons at β frequency. (A) Mean Coherence calculated during the OFF vs. ON laser stimulation between mCx ECoG and STN (blue), or arkyallidal (black) or prototypic neurons (red). (B) Box-and-whisker plots comparing the β -coherence (12-30 Hz) OFF vs. ON laser stimulation for STN (blue, n=20, AUC β -coherence OFF vs. ON: $1.6 \pm 0.2 \times 10^{-1}$ vs. $8.3 \pm 1.0 \times 10^{-1}$, paired t -test, $t=-6.67$, $p<0.001$), for arkyallidal (black, n=3, AUC β -coherence OFF vs. ON: $1.2 \pm 0.4 \times 10^{-1}$ vs. $2.8 \pm 0.5 \times 10^{-1}$), and prototypic neurons (red, n=23, AUC β -coherence OFF vs. ON: $1.8 \pm 0.1 \times 10^{-1}$ vs. $9.7 \pm 1.0 \times 10^{-1}$, paired t -test, $t=-7.74$, $p<0.001$). (C) Example of STN firing rate disinhibition induced by increasing intensity of GP opto-inhibition (scale bar: 2 mV). (D) Population PSTH of STN firing to increasing intensity of GP opto-inhibition (n=21 STN neurons, GP opto-inhibition at 2.5 mW in black, 5 mW in blue, 10 mW in green, and 15 mW in red). (E) MI of STN neurons in response to the different intensity of GP opto-inhibition (n=21, MI at 2.5 mW vs. 5 mW vs. 10 mW vs. 15 mW, $4.4 \pm 0.7 \times 10^{-1}$ vs. $5.6 \pm 0.7 \times 10^{-1}$ vs. $6.9 \pm 0.5 \times 10^{-1}$ vs. $7.5 \pm 0.5 \times 10^{-1}$, repeated measures ANOVA, $F=34.226$, $p<0.001$, following by Student-Newman-Keuls post hoc test, $p<0.001$ for 2.5 mW vs. 5 mW, 2.5 mW vs. 10 mW, 2.5 mW vs. 15 mW, 5 mW vs. 10 mW, 5 mW vs. 15 mW, $q= 5.0, 10.5, 13.2, 5.5$ and 8.1 respectively).

Figure S10

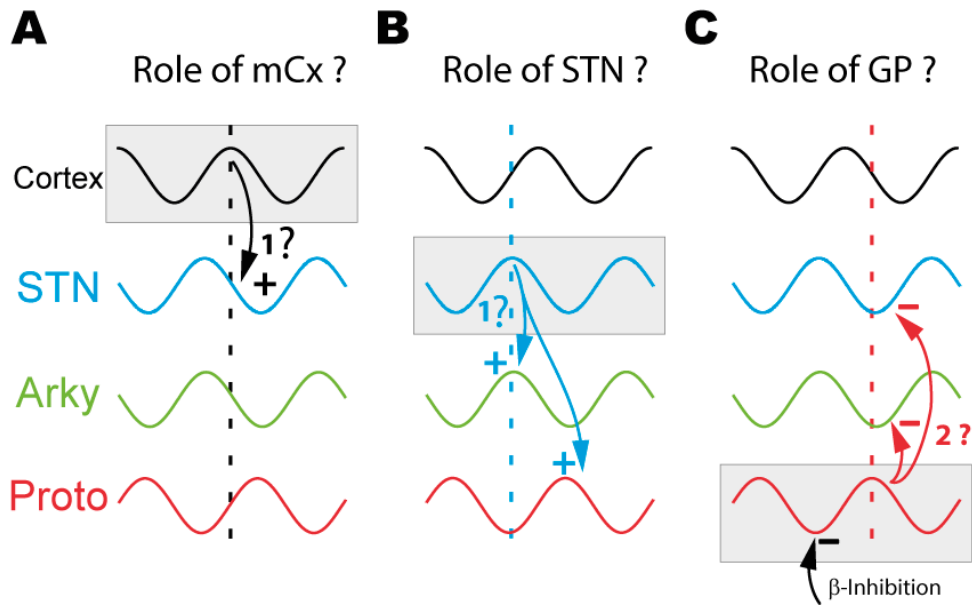


Figure S10. Circuit mechanisms driving β -oscillations in parkinsonism. (A-C) Schematic representation of the neuronal β -oscillatory activity in cortico-basal ganglia circuits illustrating the various mechanism of β -generation that we have tested in this work. (A) The motor cortex (mCx) has been proposed to drive β -oscillatory activity in basal ganglia circuit, possibly through the hyperdirect pathway that directly inputs excitation at the level of the STN. We demonstrate in this work that opto-inhibition of the cortex or decortication experiments have no effect on the generation/propagation of β -oscillations. (B) Another hypothesis involves the activity of STN neurons to drive β -oscillatory activity in globus pallidus neurons and the rest of basal ganglia. However, we show here that STN opto-inhibition and electrolytic lesion do not affect the level of β -oscillations expression in these circuits. In addition, reintroduction of artificial β -oscillations in the STN did not reproduce the functional properties of parkinsonian β -oscillations. (C) The last hypothesis we tested in this study was the contribution of GP activity to β -rhythm generation/propagation. Our results indicate that β -activity is dependent on GP neurons and driven through inhibitory mechanisms. The inhibitory drive is likely coming from striatal indirect neurons⁴³ that might preferentially impact onto prototypic neurons. Our work supports the view that GP neurons, and especially prototypic neurons, are critical for the orchestration and the broadcasting of β -rhythm to STN and cortico-basal ganglia circuits. Abbreviations: mCx: motor cortex, STN: subthalamic nucleus, GP: globus pallidus, Arky: arkypallidal neurons, Proto: prototypic neurons.

ONLINE METHODS

Animals

All Experimental procedures were performed on adult male Sprague-Dawley rats (9 to 21 weeks, Janvier Labs) in accordance with the European legislation for the protection of animals used for scientific purposes (directive 2010/63/EU). This project was also approved by the French ministry of higher education and research and the ethical committee of CNRS, Aquitaine Region (accreditation number 5012079-A). Rats were housed collectively (at least by 2) per cage under artificial conditions of light (light/dark cycle, light on at 7:00 a.m.), temperature (24°C), and humidity (45%) with food and water available ad libitum. A total number of 93 rats were used for this study of which 20 rats were excluded due to the low transduction rate of STN neurons as verified with electrophysiological recordings in STN (see 'Functional optogenetic mapping of laser effect in STN' for more details).

Stereotaxic injection of 6-hydroxydopamine

Unilateral 6-hydroxydopamine (6-OHDA) lesions were induced as previously described¹⁰. Briefly, rats (300-350 g) were anesthetized with isoflurane (induction/maintenance: 3-5/1.5%; Iso-vet®, Piramal healthcare), fixed on a stereotaxic frame (Unimécanique, M2e) and placed on heating blanket. An ophthalmic ointment (Liposic®, Bauch & Lomb Swiss) was used all along the surgery to prevent dehydration. Then, the rats received desipramine hydrochloride (25 mg/Kg, i.p; CAT#D3900, Sigma-Aldrich) thirty minutes before 6-OHDA injection in the right medial forebrain bundle (AP, -3.8 mm caudal to bregma; ML, 1.6 mm from midline, Paxinos and Watson 2007). This pre-treatment was used to prevent noradrenergic system lesion⁸⁹. After subcutaneous injection of xylocaine (15 mg/Kg; AstraZeneca), skull was exposed and a craniotomy was performed to inject 2.5 µL of 6-OHDA 3% (w/v; CAT#162957, Sigma-Aldrich) solution. This latter was dissolved in saline solution containing ascorbic acid 0.1% (w/v; CAT#A4544, Sigma-Aldrich) and was injected in five points (500 nL each) separated by 250 µm vertical intervals (-7 to -8 mm from cortical surface) with glass capillary (tip diameter 35 µm; 1-5 µL Hirschmann® microcapillary pipette, CAT#Z611239, Sigma-Aldrich) connected to Picospritzer® (Parker Hannifin). At the end of surgery, 5.5% glucose solution (w/v; CAT#G8270, Sigma-Aldrich) and buprenorphine (0.05 mg/Kg; Axience) were injected subcutaneously. To assess the 6-OHDA lesion, an apomorphine challenge was performed (0.05 mg/kg, s.c.; Apokinin®, Aguetant) 14-15 days after surgery (Schwartz and Huston 1996; Mallet et al. 2008; Mallet et al. 2008). Only rats performing 80 net rotations in 20 minutes were selected in this study.

Stereotaxic injection of viral vectors

All the virus used for our optogenetic manipulations were adeno-associated virus directly purchased from a vector core (UNC vector core) and micro-injected under stereotaxic condition in control or hemi-lesioned rats using glass capillary (tip diameter 35 μm ; 1-5 μL Hirschmann® microcapillary pipette, CAT#Z611239, Sigma-Aldrich) connected to a Picospritzer® pressure system (Parker Hannifin). All injections were performed under the same surgical methodology as described before. Experiments of mCx optogenetic inhibition, were achieved using an AAV2/5-CamKIIa-eArchT3-YFP viral vector (3×10^{12} viral particles/mL) injected in rats ($n=13$, total volume of 2 μL) injected in 4 points of the M1/M2 mCx ipsilaterally to the lesion (500 nL per injection sites at coordinates: AP, +4 mm rostral to bregma, ML, +2 and +2.8 mm from midline; AP, +3.4 mm rostral to bregma, ML, +1.8 and +2.6 from midline; DV, -1.5 mm from cortical surface, Paxinos and Watson 2007). For STN manipulations, we injected in hemi-lesioned (ipsilateral to lesion) or normal animals (right hemisphere) the viral solutions AAV2/5-CamKII-eArchT3-YFP ($n=13$ hemi-lesioned rats, 3×10^{12} viral particles/mL), AAV5-hSyn-eArch3-YFP ($n=9$ hemi-lesioned rats, 3×10^{12} viral particles/mL), or AAV2/5-CamKIIa-hChR2(H134R)-YFP ($n=7$ and 10 for hemi-lesioned and normal animals respectively, 6.2×10^{12} viral particles/mL) in 2 injection points in the STN (250 nL each, coordinates: AP, -3.6 and -3.9 mm caudal to bregma, ML, +2.5 mm from midline, DV, -7.5 mm from cortical surface, Paxinos and Watson 2007). For GP optogenetic inhibition, we used an AAV2/5-hSyn-eArch3-YFP (3×10^{12} viral particles/mL, 600 nL injected in 2 injections points, 300 nL each, coordinates: AP, -0.9 mm caudal to bregma, ML, +2.8 mm from midline, DV, -5.6 and 6.1 mm from cortical surface, Paxinos and Watson 2007) in GP of hemi-lesioned ($n=15$, ipsilateral to lesion) or control ($n=18$, right hemisphere) animals.

In vivo electrophysiological recording

Electrophysiological recordings and optogenetic manipulations were realized at least 4 weeks after viral transduction under urethane anaesthesia. Anaesthesia was first induced with isoflurane (3-5%; Iso-vet®, Piramal healthcare), and maintained with urethane (i.p., 1.3 g/Kg.; CAT#U2500, Sigma-Aldrich). The animals were then secured in a stereotaxic frame (Unimécanique, M2e) and placed on heating blanket. After subcutaneous injection of xylocain, skull was exposed and craniotomies were performed to enable electrophysiological recordings and optogenetic stimulation of the region of interest (same stereotaxic coordinates as above). In each rat, an electrocorticogram (ECoG) of the sensorimotor cortex were realized (AP, +4.3 mm rostral to bregma; ML, +2 mm from midline, Paxinos and Watson 2007) with a

Imm-screw juxtaposed to the dura mater (Mallet et al. 2008; Mallet et al. 2008; Mallet et al. 2012). All along the recording session, saline solution was used to prevent dehydration and anaesthesia level was frequently controlled by examination of ECoG and by testing the response to light sensory stimuli (tail pinch).

In vivo extracellular recordings were performed using glass electrodes (1-3 μm tip end, 12-20 $\text{M}\Omega$, GC150F, WPI) filled with a chloride solution 0.5 M containing neurobiotin tracer (1-2%, w/v; CAT#SP-1120, Vector laboratories) to perform juxtacellular labelling as described below^{27,91}. For GP recordings, neurons were classified as prototypic and arky pallidal neurons based on their well-known electrophysiological signature across different brain-state^{27,41}. A subset of neurons (n=10) were further labelled with neurobiotin and identified according to their molecular profiles: prototypic neurons expressed the transcription factor Nkx2.1 whereas arky pallidal neurons expressed the transcription factor FoxP2. Optogenetic manipulation of the recorded neurons were performed using an opto-electrode that was homemade by gluing an optical fibers (multimode Fiber, 0.22 NA, core diameter: 105 μm , Thorlabs) 1 mm and/or 2 mm above the tip of the glass recording electrodes. This method allows extracellular recording during opto-manipulation and juxtacellular labelling. Once the opto-electrode was implanted in the recording structure, the signal was amplified 10 fold using an axoClamp 2B (in bridge mode; Molecular Devices). The recorded signal was then amplified 1000 fold and filtered using a differential AC amplifier (spike unit: 0.3 Hz-10 kHz, LFP: 0.1 Hz-10 kHz; model 1700, A-M Systems). For ECoG recording, the signal was amplified 1000 fold and filtered with the same differential AC amplifier (0.1 Hz-5 kHz). Finally, all recorded signals were digitalized at 20 kHz, by using the Power1401-3 connected to a computer equipped with Spike2 software (Cambridge Electronic Design). To facilitate the identification of STN during the recording sessions, a concentric bipolar electrode (SNEX-100, Rhodes Medical Instruments) connected to an isolated stimulator (DS3 Isolated Current Stimulator, Digitimer), was inserted in the mCx (coordinates: AP, +3.5 mm rostral to bregma, ML, +3.5 mm from midline, DV, -1.8 mm from cortical surface, Paxinos and Watson 2007). STN was identified by checking online the STN response to mCx electrical stimulation as previously described⁹². We then validated the recording location with histological control, in particular the location of the juxtacellularly-labelled neurons and the track marks left by the opto-electrode.

Functional optogenetic mapping of laser effect in STN

In order to validate the results of our STN opto-inhibition and STN opto-excitation experiments performed in 6-OHDA rats, it was critical to verify functionally that the overall level of optical control achieved in STN was acceptable. For this reason, we adopted an opto-

electrode mapping strategy that consisted of combining laser stimulation with STN extracellular recordings at multiple locations in the STN (i.e. at least 3 penetrations spaced by 150 μm in the antero-posterior or medio-lateral axis of the STN). In addition, only animals that had at least 10 STN cells opto-tested *in vivo* and presenting >60% of significantly laser-modulated cells were kept for further analysis. Using these criteria, hemi-lesioned animals with poor STN optogenetic control were excluded from the study, that is: 9 out of 13 rats injected with AAV5-CamKII-eArch3-EYFP; 5 out of 9 injected with AAV5-hSyn-eArch3-EYFP; and 2 out of 7 injected with AAV5-CamKII-ChR2-EYFP. The level of STN optical control was also verified/quantified in normal animals injected with an AAV5-CamKII-ChR2-EYFP (4 out of 10 excluded) or with the AAV5-CamKII-eArchT3.0-EYFP (none excluded out of 4).

Optogenetic stimulation

To apply optogenetic stimulation, we implanted optical fibers (multimode Fiber, 0.22 NA, core diameter: 105 μm , Thorlabs) into the GP (coordinates: AP, -0.9 mm caudal to bregma, ML, +2.8 mm from midline, DV, -5.6 and 6.1 mm from cortical surface, Paxinos and Watson 2007) or STN (coordinates: AP, -3.7 mm to bregma, ML, +2.5 mm from midline, DV, -7.0 mm from cortical surface, Paxinos and Watson 2007) or mCx. Note that for mCx inhibition, 2 optic fibers were implanted to maximize the volume of cortical inhibition (coordinates: AP, +4 mm rostral to bregma, ML, +2.2 mm from midline; AP, +3.4 mm rostral to bregma, ML, +2.2 mm from midline; DV, -1.0 mm from cortical surface, Paxinos and Watson 2007). The power at the tip of the optics fibers was always measured with a power meter (PM100D, Thorlabs) right before insertion in brain tissue. Two optogenetic stimulation protocols were used in this study. The first one consisted of 2 s of continuous yellow or blue light (15 or 2.5 mW at the tip of optical fiber respectively) every 10 s. The 2 s preceding the light pulse was used as baseline (OFF period) to compare the effect of the 2 s of optogenetic manipulation (ON epoch). Only recordings that contained a minimum of 30 laser stimulations (and at least 60 s during OFF and ON epochs) were kept for analyses to quantify the effect of the optogenetic inhibitions on β -synchronization (phase locking, ECoG power and coherence). For each animal, the best β -oscillations recording was determined based on the highest peak in the β -AUC (12-30 Hz) power spectrum calculation. The effect of our optogenetic manipulations on the neuronal firing rate measured in STN and GP neurons (in hemi-lesioned and control animals) were determined using at least 10 laser stimulations. To reintroduce abnormal β -synchronization in control animal, we used a different protocol that consisted of 20 s of sinusoidal yellow or blue light stimulation (15 or 2.5 mW at the tip of optical fiber,

respectively). Only the positive part of the sinusoid drove laser activation. The baseline OFF epoch consisted of the 20 s before light stimulation and was compared to the ON epoch that contains 20 s of sinusoidal stimulation. Only recording with at least 3 sinusoidal protocols (60 s) were included in this study. The laser diode (Errol laser) was controlled by an analogic signals sent by a Power1401-3 (Cambridge Electronic Design) and controlled with the Spike2 software (Cambridge Electronic Design).

Decortication experiments and STN electrolytic lesion

To test the importance of other cortical area in the generation mechanism of β -oscillations we performed large-scale decortication experiments. Removal of the temporal and frontal bones exposed most of the dorsal cortical surface. We removed the cortical tissue using an electrosurgical cautery (BC 50D, Anhui Yingte Electronic) and the depth of the lesion was assessed based on the visual inspection of the corpus callosum. As shown in supplementary Figure S2, this approach allowed to lesion a broad cortical volume including the M1, M2, S1 and a large part of the S2 cortex. In these experiments, brain state activity was monitored through an ECoG recorded above mCx on the contralateral side of the lesion and combined with GP LFP recording (ipsilateral to lesion) using 32-channel silicon probe microelectrodes (Cambridge Neurotech, GB) in anaesthetized hemi-lesioned rats (n=3).

To further test the contribution of STN in generating β -oscillations, we performed an electrolytic lesion of the STN in anaesthetized hemi-lesioned rats (n=3). We first performed electrophysiological recordings to map the exact stereotaxic location and depth of the STN. We then lowered a concentric bipolar electrode (SNEX-100, Rhodes Medical Instruments) and located the tip of the electrode at the bottom of the STN. The electrode was connected to an isolated stimulator (DS3 Isolated Current Stimulator, Digitimer) and an electrolytic lesion was performed by applying a continuous current (3 mA during 20 s) in two stereotaxic coordinates separated by 300 μm in the rostro-caudal axis. Ipsilateral ECoG recording was performed before and after STN lesion.

Juxtacellular stimulation

In this study, we performed juxtacellular labelling to identify the location/cell-type of the recorded unit in STN or in GP. Briefly, the recorded unit was stimulated by a current pulse of 250 ms long (50 % duty cycle, 1-10 nA) sent through the recording electrode by axoClamp 2B (in bridge mode; Molecular Devices). Only recording with at least 250 stimulations were included in this study.

Data processing and analysis

We performed simultaneous recording of the mCx ECoG and STN unit activity at a sampling rate of 20kHz during epoch containing β -synchronization. All data processing (spike sorting and ECoG filtering) were realized offline with Spike2 software (Cambridge Electronic Design). The ECoG signal was high-pass filtered at 0.5Hz (DC remove) and low-pass filtered at 500 Hz following by a down-sampling at the same frequency (to avoid aliasing effect) for further field analysis. The frequency resolution was set at around 1 Hz (FFT size = 500/512 Hz) to analyse the root mean square ECoG power spectrum or to calculate the coherence between spike train and ECoG (using “coher” script, freely available on CED website). For generating perievent spectrograms, we computed in Matlab® R2016a (MathWorks, **Natick, MA, USA**) using the `ft_freqanalysis` function (time/frequency slide windows: 50 ms /0.071 Hz, cycle number: 7) of the Fieldtrip toolbox⁹³. Peri-stimulus time histograms or PSTH (width: 6 s, offset: 2 s, bin size: 50 ms) of each spike trains were generated using spike2 and a custom Matlab® script. Both frequency and count PSTH were generated for each spike train to evaluate the effect of the optogenetic manipulations. A response was classified as statistically significant if the spike count values of 3 consecutive bins within the first 400 ms of light pulse delivery were $< -2SD$ (inhibitory response) or $> 2SD$ (excitatory response). SD was measured during OFF epoch. We also analysed in spike2 the frequency of each spike train during OFF and ON epoch. This allowed us to calculate the modulatory index or MI⁹⁴ for evaluating the frequency increasing induced by our manipulations. MI was calculated as follow: $(\text{frequency ON} - \text{frequency OFF}) / (\text{frequency ON} + \text{frequency OFF})$.

To generate the linear phase histograms in spike2 (bin size: 10°), we detected the peak of β -oscillations in the band-pass filtered (12-30 Hz) ECoG using a threshold detection as previously described (Mallet et al. 2008; Mallet et al. 2012). The linear phase histograms were then transferred to Matlab® for further analysis using circular statistics toolbox⁹⁵. To determine if a spike activity was significantly modulated by the β -oscillations measured in the ECoG, we performed the Rayleigh test for circular uniformity using the ‘`circ_rtest`’ function which evaluates if the spike unit activity is uniformly distributed across the ECoG β -oscillation cycles (H_0 , $p > 0.05$). If H_0 was rejected, neuron was considered as significantly entrained by β -oscillations. The mean angle and vector length for each spike train were also measured by using the ‘`circ_mean`’ and ‘`circ_r`’ function, respectively. Finally, the mean angles of entrained neurons were compared (OFF vs. ON epoch or between groups) by using the Watson-Williams F test (‘`circ_wwtest`’ function, circular statistics toolbox).

Random spike removing in mCx experiment

Our mCx optogenetic inhibition was associated with a reduction in the firing rate of STN neurons and a consequent decrease in the coherence value measured between STN spike and ECoG reduction in the functional connectivity. To determine the influence of change in firing rate on the spike-ECoG coherence value we performed random spike removal on our STN spike timestamps using the 'randsample' Matlab® function. We analysed the effect of a 20% or 50% decrease in STN firing rate and performed coherence analysis in Spike2 as previously described.

Effect of optogenetic stimulation across β -oscillations power distribution

To analyse the effect of the optogenetic stimulation across the β -power distribution, we compared the root mean square power of every individual β oscillations period as measured through the area under the curve (AUC) within the 12-30 Hz frequency band for each stimulation epoch (OFF laser vs. ON laser) for each neuron. The β -AUC was calculated in Matlab® through an interpolation method ('interp1' function) of the power spectrum in the 12 to 30 Hz frequency band. A β -AUC difference (β -AUC above interpolated line) - (β -AUC below interpolated line) was calculated for every 2 s long stimulation epoch (OFF and ON laser stimulation). Finally, the cumulative distribution was computed with the 'cdfplot' function (Matlab®).

Beta bursts detection

The β bursts were extracted from the ECoG signal recorded above the mCx and according to a threshold detection method previously published⁹⁶. The signal was first down sampled at 500 Hz and band-pass filtered in the β -band (see Data processing and analysis). The filtered ECoG signal was then imported into Matlab and the envelope of the β signal was calculated using the hilbert() function. The signal was defined as a beta burst if: 1/ the amplitude of the envelope exceeding the 75th percentile threshold of the analytic signal measured during the entire recording, and 2/ the duration of the burst was longer than 50 ms. Finally, the duration and the number of β -bursts were averaged accordingly to the 3 laser epochs (i.e. Before, OFF and ON) and statistically compared.

Tissue processing and histological control

At this end of recording day, the rats were sacrificed with an overdose of pentobarbital sodium (150 mg/Kg, i.p.; Axience). An intracardiac perfusion (PBS 0.01mM following by formaldehyde 4%) was then performed for further histological validations. The brain was kept overnight in a solution of PBS 0.01 mM / formaldehyde 4% (v/v; CAT#20909.330, VWR) and then cut in 50 μ m slices with a vibratome (VT1000, Leica Microsystems). To reveal the juxtacellularly labelled neurons, the slices were incubated overnight in a solution of PBS 0.01

mM / Triton™ X100 0.3% (v/v; CAT#T9284, Sigma-Aldrich) containing streptavidine-CY3 Zymax (1/1000, v/v; CAT#438315, Life Technologies). The slices were then washed in PBS 0.01 mM before mounting onto slides in vectashield medium (CAT#H-1000, Vector laboratories). Additional staining was performed through indirect immunofluorescence staining using primary and fluorescent secondary antibodies. For all immunostainings, the slices were incubated overnight in a solution of PBS 0.01mM / Triton™ X100 0.3% (v/v) containing the primary antibody. The slices were then washed 3 times in PBS 0.01 mM, incubated 4h in a solution of PBS 0.01 mM / Triton™ X100 0.3% (v/v) containing the secondary antibody, washed again in PBS 0.01 mM and mounted onto slides in vectashield medium (CAT#H-1000, Vector laboratories). The primary antibodies used in this study were: chicken anti-YFP (1/1000, v/v; CAT#GFP-1020, Avès labs), rabbit anti-Nkx2.1 (or anti-TTF-1, prototypic neuron labelling, 1/500, v/v; CAT#H-190, Santa Cruz) and goat anti-FoxP2 (arkypallidal neuron labelling, 1/500, v/v; CAT#N-16, Santa Cruz). The secondary antibodies used were: Alexa Fluor® 488 donkey anti-chicken (1/500, v/v; CAT#703-545-155, Jackson ImmunoResearch), CY™5-conjugated donkey anti-rabbit (1/500, v/v; CAT#711-175-152, Jackson ImmunoResearch), and Brilliant Violet™421-conjugated donkey anti-goat (1/500, v/v; CAT#705-675-147, Jackson ImmunoResearch). The images were acquired with a fluorescence microscope (Axio Imager 2, Zeiss) or a confocal microscope (Leica, SP8) and were analysed with Fiji (ImageJ 1.52)⁹⁷. To determine if our opto-mapping recordings applied to STN opto-inhibition experiments in parkinsonian rats accurately capture the level of STN infection (Figure S3A, B), we performed an histological quantification of the effectiveness and spread of virus infection in the STN. To do so, we determined the intensity of STN fluorescence in the EYFP channel using Region of Interest (ROI) measures in Fiji. Briefly, we mounted serial brain sections spaced by 300 µm and containing STN sagittal slices at different medio-lateral coordinate (i.e. 2.9/2.6/2.3/2 mm from the midline). For each slices, the value of ROI was normalized according to the background labelling in a region devoid of EYFP signal and taken just below the STN region. For each rat, we averaged the different STN ROI values and correlated this measure to the percentage of opto-inhibition as determined by our opto-mapping strategy.

Statistical Analysis

The statistical analyses were performed using SigmaPlot 12 (Systat Software). For independent samples, we applied the normality (Shapiro-Wilk test) and equal variance tests. A *t*-test was used if the distributions were normal and the group variances were equal. Otherwise, the Mann-Whitney signed rank test was used. In a same way, Kruskal-Wallis one

way ANOVA was used instead of one way ANOVA, when normality distributions and variance homogeneity were not verified. ANOVA was followed by Student-Newman-Keuls post hoc test. For dependant sample, the paired *t*-test was used excepts if the normality distribution test failed (Shapiro-Wilk test, $p < 0.05$). In the latter case, the Wilcoxon signed rank test was used. In same way, Friedman repeated measures ANOVA on ranks was used instead of one way repeated measure ANOVA, when normality distribution was not verified. ANOVA repeated measure was followed by Holm-Sidak (parametric) or Dunn's (non-parametric) post hoc test.

Data and Code Availability

The data that support the findings and the code for the analysis are available from the corresponding author upon request.

References

1. Ainsworth, M. *et al.* Rates and Rhythms: A Synergistic View of Frequency and Temporal Coding in Neuronal Networks. *Neuron* **75**, 572–583 (2012).
2. Schoffelen, J. M., Oostenveld, R. & Fries, P. Neuronal coherence as a mechanism of effective corticospinal interaction. *Science (80-.)*. **308**, 111–113 (2005).
3. Uhlhaas, P. J. & Singer, W. Neural Synchrony in Brain Disorders: Relevance for Cognitive Dysfunctions and Pathophysiology. *Neuron* **52**, 155–168 (2006).
4. DeLong, M. R. Primate models of movement disorders of basal ganglia origin. *Trends Neurosci.* **13**, 281–285 (1990).
5. Albin, R. L., Young, A. B. & Penney, J. B. The functional anatomy of basal ganglia disorders. *Trends Neurosci.* **12**, 366–75 (1989).
6. Hutchison, W. D. Neuronal Oscillations in the Basal Ganglia and Movement Disorders: Evidence from Whole Animal and Human Recordings. *J. Neurosci.* **24**, 9240–9243 (2004).
7. Raz, A., Vaadia, E. & Bergman, H. Firing patterns and correlations of spontaneous discharge of pallidal neurons in the normal and the tremulous 1-methyl-4-phenyl-1,2,3,6-tetrahydropyridine vervet model of parkinsonism. *J. Neurosci.* **20**, 8559–71 (2000).

8. Bergman, H. *et al.* Physiological aspects of information processing in the basal ganglia of normal and parkinsonian primates. *Trends Neurosci.* **21**, 32–38 (1998).
9. Plotkin, J. L. & Goldberg, J. A. Thinking Outside the Box (and Arrow): Current Themes in Striatal Dysfunction in Movement Disorders. *Neurosci.* **25**, 359–379 (2019).
10. Mallet, N., Ballion, B., Le Moine, C. & Gonon, F. Cortical inputs and GABA interneurons imbalance projection neurons in the striatum of parkinsonian rats. *J. Neurosci.* **26**, 3875–3884 (2006).
11. Parker, J. G. *et al.* Diametric neural ensemble dynamics in parkinsonian and dyskinetic states. *Nature* **557**, 177–182 (2018).
12. Kravitz, A. V *et al.* Regulation of parkinsonian motor behaviours by optogenetic control of basal ganglia circuitry. *Nature* **466**, 622–6 (2010).
13. Sharott, A. *et al.* Activity Parameters of Subthalamic Nucleus Neurons Selectively Predict Motor Symptom Severity in Parkinson’s Disease. *J. Neurosci.* **34**, 6273–6285 (2014).
14. Sanders, T. H., Clements, M. A. & Wichmann, T. Parkinsonism-related features of neuronal discharge in primates. *J. Neurophysiol.* **110**, 720–731 (2013).
15. Hutchison, W. D. *et al.* Neuronal oscillations in the basal ganglia and movement disorders: evidence from whole animal and human recordings. *J. Neurosci.* **24**, 9240–3 (2004).
16. Stein, E. & Bar-Gad, I. B Oscillations in the Cortico-Basal Ganglia Loop During Parkinsonism. *Exp. Neurol.* **245**, 52–9 (2013).
17. Hammond, C., Bergman, H. & Brown, P. Pathological synchronization in Parkinson’s disease: networks, models and treatments. *Trends Neurosci.* **30**, 357–364 (2007).
18. Neumann, W.-J. *et al.* Subthalamic synchronized oscillatory activity correlates with motor impairment in patients with Parkinson’s disease. *Mov. Disord.* **31**, 1748–1751 (2016).
19. Little, S., Pogosyan, A., Kuhn, A. A. & Brown, P. Beta band stability over time correlates with Parkinsonian rigidity and bradykinesia. *Exp. Neurol.* **236**, 383–388

- (2012).
20. Ermentrout, B., Pascal, M. & Gutkin, B. The effects of spike frequency adaptation and negative feedback on the synchronization of neural oscillators. *Neural Comput.* **13**, 1285–1310 (2001).
 21. Pavlides, A., Hogan, S. J. & Bogacz, R. Computational Models Describing Possible Mechanisms for Generation of Excessive Beta Oscillations in Parkinson’s Disease. *PLoS Comput. Biol.* **11**, e1004609 (2015).
 22. Rubin, J. E. Computational models of basal ganglia dysfunction: the dynamics is in the details. *Curr. Opin. Neurobiol.* **46**, 127–135 (2017).
 23. Shouno, O., Tachibana, Y., Nambu, A. & Doya, K. Computational Model of Recurrent Subthalamo-Pallidal Circuit for Generation of Parkinsonian Oscillations. *Front. Neuroanat.* **11**, 1–15 (2017).
 24. Plenz, D. & Kital, S. T. A basal ganglia pacemaker formed by the subthalamic nucleus and external globus pallidus. *Nature* **400**, 677–682 (1999).
 25. Bevan, M. Move to the rhythm: oscillations in the subthalamic nucleus–external globus pallidus network. *Trends Neurosci.* **25**, 525–531 (2002).
 26. Mallet, N. *et al.* Parkinsonian beta oscillations in the external globus pallidus and their relationship with subthalamic nucleus activity. *J. Neurosci.* **28**, 14245–14258 (2008).
 27. Mallet, N. *et al.* Dichotomous organization of the external globus pallidus. *Neuron* **74**, 1075–86 (2012).
 28. Brittain, J. S. & Brown, P. Oscillations and the basal ganglia: Motor control and beyond. *Neuroimage* **85**, 637–647 (2014).
 29. McCarthy, M. M. *et al.* Striatal origin of the pathologic beta oscillations in Parkinson’s disease. *Proc. Natl. Acad. Sci.* **108**, 11620–11625 (2011).
 30. Leblois, A., Boraud, T., Meissner, W., Bergman, H. & Hansel, D. Competition between feedback loops underlies normal and pathological dynamics in the basal ganglia. *J. Neurosci.* **26**, 3567–83 (2006).
 31. Corbit, V. L. *et al.* Pallidostriatal Projections Promote Beta Oscillations in a

- Dopamine-Depleted Biophysical Network Model. *J. Neurosci.* **36**, 5556–5571 (2016).
32. Steriade, M. Grouping of brain rhythms in corticothalamic systems. *Neuroscience* **137**, 1087–1106 (2006).
 33. Jones, E. G. Synchrony in the interconnected circuitry of the thalamus and cerebral cortex. *Ann. N. Y. Acad. Sci.* **1157**, 10–23 (2009).
 34. Li, Q. *et al.* Therapeutic deep brain stimulation in Parkinsonian rats directly influences motor cortex. *Neuron* **76**, 1030–41 (2012).
 35. Nambu, A. & Tachibana, Y. Mechanism of parkinsonian neuronal oscillations in the primate basal ganglia: some considerations based on our recent work. *Front. Syst. Neurosci.* **8**, 74 (2014).
 36. Mallet, N. *et al.* Disrupted dopamine transmission and the emergence of exaggerated beta oscillations in subthalamic nucleus and cerebral cortex. *J. Neurosci.* **28**, 4795–4806 (2008).
 37. Lepage, K. Q., Kramer, M. A. & Eden, U. T. The dependence of spike field coherence on expected intensity. *Neural Comput.* **23**, 2209–2241 (2011).
 38. Deffains, M. *et al.* Subthalamic, not striatal, activity correlates with basal ganglia downstream activity in normal and parkinsonian monkeys. *Elife* **5**, 1–38 (2016).
 39. Gradinaru, V., Mogri, M., Thompson, K. R., Henderson, J. M. & Deisseroth, K. Optical Deconstruction of Parkinsonian Neural Circuitry. *Science (80-.)*. **324**, 354–359 (2009).
 40. Kita, H. & Kitai, S. T. Intracellular study of rat globus pallidus neurons: membrane properties and responses to neostriatal, subthalamic and nigral stimulation. *Brain Res.* **564**, 296–305 (1991).
 41. Mallet, N. *et al.* Arky pallidal Cells Send a Stop Signal to Striatum. *Neuron* **89**, 308–316 (2016).
 42. Abdi, A. *et al.* Prototypic and Arky pallidal Neurons in the Dopamine-Intact External Globus Pallidus. *J. Neurosci.* **35**, 6667–6688 (2015).
 43. Sharott, A., Vinciati, F., Nakamura, K. C. & Magill, P. J. A population of indirect

- pathway striatal projection neurons is selectively entrained to parkinsonian beta oscillations. *J. Neurosci.* **37**, 0658–17 (2017).
44. Brown, P. Abnormal oscillatory synchronisation in the motor system leads to impaired movement. *Curr. Opin. Neurobiol.* **17**, 656–664 (2007).
 45. Fogelson, N. *et al.* Different functional loops between cerebral cortex and the subthalamic area in parkinson's disease. *Cereb. Cortex* **16**, 64–75 (2006).
 46. Williams, D. *et al.* Dopamine-dependent changes in the functional connectivity between basal ganglia and cerebral cortex in humans. *Brain* **125**, 1558–69 (2002).
 47. Litvak, V. *et al.* Resting oscillatory cortico-subthalamic connectivity in patients with Parkinson's disease. *Brain* **134**, 359–374 (2011).
 48. Lalo, E. *et al.* Patterns of Bidirectional Communication between Cortex and Basal Ganglia during Movement in Patients with Parkinson Disease. *J. Neurosci.* **28**, 3008–3016 (2008).
 49. Sharott, A., Magill, P. J., Bolam, J. P. & Brown, P. Directional analysis of coherent oscillatory field potentials in the cerebral cortex and basal ganglia of the rat. *J. Physiol.* **562**, 951–63 (2005).
 50. Surmeier, D. J., Mercer, J. N. & Chan, C. S. Autonomous pacemakers in the basal ganglia: who needs excitatory synapses anyway? *Curr. Opin. Neurobiol.* **15**, 312–8 (2005).
 51. Chu, H.-Y., McIver, E. L., Kovalski, R. F., Atherton, J. F. & Bevan, M. D. Loss of Hyperdirect Pathway Cortico-Subthalamic Inputs Following Degeneration of Midbrain Dopamine Neurons. *Neuron* **95**, 1306-1318.e5 (2017).
 52. Mathai, A. *et al.* Reduced cortical innervation of the subthalamic nucleus in MPTP-treated parkinsonian monkeys. *Brain* **138**, 946–962 (2015).
 53. Sanders, T. H. & Jaeger, D. Optogenetic stimulation of cortico-subthalamic projections is sufficient to ameliorate bradykinesia in 6-ohda lesioned mice. *Neurobiol. Dis.* **95**, 225–237 (2016).
 54. Sharott, A. *et al.* Dopamine depletion increases the power and coherence of β -

- oscillations in the cerebral cortex and subthalamic nucleus of the awake rat. *Eur. J. Neurosci.* **21**, 1413–1422 (2005).
55. Leventhal, D. K. *et al.* Basal Ganglia Beta Oscillations Accompany Cue Utilization. *Neuron* **73**, 523–536 (2012).
56. Rubino, D., Robbins, K. A. & Hatsopoulos, N. G. Propagating waves mediate information transfer in the motor cortex. *Nat. Neurosci.* **9**, 1549–1557 (2006).
57. Gilbertson, T. *et al.* Existing motor state is favored at the expense of new movement during 13-35 Hz oscillatory synchrony in the human corticospinal system. *J. Neurosci.* **25**, 7771–9 (2005).
58. Engel, A. K. & Fries, P. Beta-band oscillations-signalling the status quo? *Curr. Opin. Neurobiol.* **20**, 156–165 (2010).
59. Mirzaei, A. *et al.* Sensorimotor Processing in the Basal Ganglia Leads to Transient Beta Oscillations during Behavior. *J. Neurosci.* **37**, 11220–11232 (2017).
60. Deffains, M., Iskhakova, L., Katabi, S., Israel, Z. & Bergman, H. Longer β oscillatory episodes reliably identify pathological subthalamic activity in Parkinsonism. *Mov. Disord.* **33**, 1609–1618 (2018).
61. Bergman, H., Wichmann, T., Karmon, B. & DeLong, M. R. The primate subthalamic nucleus. II. Neuronal activity in the MPTP model of parkinsonism. *J. Neurophysiol.* **72**, 507–20 (1994).
62. Shink, E., Bevan, M. D., Bolam, J. P. & Smith, Y. The subthalamic nucleus and the external pallidum: two tightly interconnected structures that control the output of the basal ganglia in the monkey. *Neuroscience* **73**, 335–357 (1996).
63. Baufreton, J., Atherton, J. F., Surmeier, D. J. & Bevan, M. D. Enhancement of excitatory synaptic integration by GABAergic inhibition in the subthalamic nucleus. *J. Neurosci.* **25**, 8505–17 (2005).
64. Bevan, M. D., Wilson, C. J., Bolam, J. P. & Magill, P. J. Equilibrium potential of GABA(A) current and implications for rebound burst firing in rat subthalamic neurons in vitro. *J. Neurophysiol.* **83**, 3169–72 (2000).

65. Gittis, A. H. *et al.* Rapid target-specific remodeling of fast-spiking inhibitory circuits after loss of dopamine. *Neuron* **71**, 858–868 (2011).
66. Chu, H.-Y., Atherton, J. F., Wokosin, D., Surmeier, D. J. & Bevan, M. D. Heterosynaptic Regulation of External Globus Pallidus Inputs to the Subthalamic Nucleus by the Motor Cortex. *Neuron* 1–13 (2015). doi:10.1016/j.neuron.2014.12.022
67. Tanimura, A., Du, Y., Kondapalli, J., Wokosin, D. L. & Surmeier, D. J. Cholinergic Interneurons Amplify Thalamostriatal Excitation of Striatal Indirect Pathway Neurons in Parkinson’s Disease Models. *Neuron* **101**, 444-458.e6 (2019).
68. Paz, J. T., Deniau, J.-M. & Charpier, S. Rhythmic bursting in the cortico-subthalamo-pallidal network during spontaneous genetically determined spike and wave discharges. *J. Neurosci.* **25**, 2092–101 (2005).
69. Alexander, G. E. & Crutcher, M. D. Functional architecture of basal ganglia circuits: neural substrates of parallel processing. *Trends Neurosci.* **13**, 266–271 (1990).
70. Kita, H. Globus pallidus external segment. *Prog. Brain Res.* **160**, 111–33 (2007).
71. Gittis, A. H. *et al.* New Roles for the External Globus Pallidus in Basal Ganglia Circuits and Behavior. *J. Neurosci.* **34**, 15178–15183 (2014).
72. Mastro, K. J. *et al.* Cell-specific pallidal intervention induces long-lasting motor recovery in dopamine-depleted mice. *Nat. Neurosci.* **20**, 815–823 (2017).
73. Mastro, K. J., Bouchard, R. S., Holt, H. a K. & Gittis, A. H. Transgenic mouse lines subdivide external segment of the globus pallidus (GPe) neurons and reveal distinct GPe output pathways. *J. Neurosci.* **34**, 2087–99 (2014).
74. Fujiyama, F. *et al.* A single-neuron tracing study of arky-pallidal and prototypic neurons in healthy rats. *Brain Struct. Funct.* **221**, 4733–4740 (2016).
75. Fan, K. Y., Baufreton, J., Surmeier, D. J., Chan, C. S. & Bevan, M. D. Proliferation of external globus pallidus-subthalamic nucleus synapses following degeneration of midbrain dopamine neurons. *J. Neurosci.* **32**, 13718–28 (2012).
76. Oorschot, D. E. Total number of neurons in the neostriatal, pallidal, subthalamic, and substantia nigral nuclei of the rat basal ganglia: A stereological study using the

- cavalieri and optical disector methods. *J. Comp. Neurol.* **366**, 580–599 (1996).
77. Koshimizu, Y., Fujiyama, F., Nakamura, K. C., Furuta, T. & Kaneko, T. Quantitative analysis of axon bouton distribution of subthalamic nucleus neurons in the rat by single neuron visualization with a viral vector. *J. Comp. Neurol.* **521**, 2125–46 (2013).
 78. Fujiyama, F. *et al.* Exclusive and common targets of neostriatofugal projections of rat striosome neurons: A single neuron-tracing study using a viral vector. *Eur. J. Neurosci.* **33**, 668–677 (2011).
 79. Kumar, A., Cardanobile, S., Rotter, S. & Aertsen, A. The Role of Inhibition in Generating and Controlling Parkinson’s Disease Oscillations in the Basal Ganglia. *Front. Syst. Neurosci.* **5**, 1–14 (2011).
 80. Terman, D., Rubin, J. E., Yew, a C. & Wilson, C. J. Activity patterns in a model for the subthalamopallidal network of the basal ganglia. *J. Neurosci.* **22**, 2963–2976 (2002).
 81. Bar-Gad, I., Heimer, G., Ritov, Y. & Bergman, H. Functional Correlations between Neighboring Neurons in the Primate Globus Pallidus Are Weak or Nonexistent. *J. Neurosci.* **23**, 4012–4016 (2003).
 82. Edgerton, J. R. & Jaeger, D. Dendritic Sodium Channels Promote Active Decorrelation and Reduce Phase Locking to Parkinsonian Input Oscillations in Model Globus Pallidus Neurons. *J. Neurosci.* **31**, 10919–10936 (2011).
 83. Bevan, M. D., Booth, P. A. C., Eaton, S. A. & Bolam, J. P. Selective Innervation of Neostriatal Interneurons by a Subclass of Neuron in the Globus Pallidus of the Rat. *J. Neurosci.* **18**, 9438–9452 (1998).
 84. Brazhnik, E., McCoy, A. J., Novikov, N., Hatch, C. E. & Walters, J. R. Ventral Medial Thalamic Nucleus Promotes Synchronization of Increased High Beta Oscillatory Activity in the Basal Ganglia-Thalamocortical Network of the Hemiparkinsonian Rat. *J. Neurosci.* **36**, 4196–4208 (2016).
 85. Tachibana, Y., Iwamuro, H., Kita, H., Takada, M. & Nambu, A. Subthalamo-pallidal interactions underlying parkinsonian neuronal oscillations in the primate basal ganglia. *Eur. J. Neurosci.* **34**, 1470–84 (2011).

86. Beck, G., Singh, A. & Papa, S. M. Dysregulation of striatal projection neurons in Parkinson's disease. *J. Neural Transm.* **125**, 449–460 (2018).
87. Liang, L., DeLong, M. R. & Papa, S. M. Inversion of Dopamine Responses in Striatal Medium Spiny Neurons and Involuntary Movements. *J. Neurosci.* **28**, 7537–7547 (2008).
88. Paxinos, G. & Watson, C. The Rat Brain in Stereotaxic Coordinates Sixth Edition. *Elsevier Acad. Press* **170**, 547–612 (2007).
89. Schwarting, R. K. W. & Huston, J. P. The unilateral 6-hydroxydopamine lesion model in behavioral brain research. Analysis of functional deficits, recovery and treatments. *Prog. Neurobiol.* **50**, 275–331 (1996).
90. Bastide, M. F. *et al.* Inhibiting Lateral Habenula Improves L-DOPA-induced Dyskinesia. *Biol. Psychiatry* **79**, 345–353 (2014).
91. Pinault, D. A novel single-cell staining procedure performed in vivo under electrophysiological control: Morpho-functional features of juxtacellularly labeled thalamic cells and other central neurons with biocytin or Neurobiotin. *J. Neurosci. Methods* **65**, 113–136 (1996).
92. Magill, P. J., Sharott, A., Bevan, M. D., Brown, P. & Bolam, J. P. Synchronous unit activity and local field potentials evoked in the subthalamic nucleus by cortical stimulation. *J. Neurophysiol.* **92**, 700–714 (2004).
93. Oostenveld, R., Fries, P., Maris, E. & Schoffelen, J. M. FieldTrip: Open source software for advanced analysis of MEG, EEG, and invasive electrophysiological data. *Comput. Intell. Neurosci.* **2011**, (2011).
94. Oldenburg, I. A. & Sabatini, B. L. Antagonistic but Not Symmetric Regulation of Primary Motor Cortex by Basal Ganglia Direct and Indirect Pathways. *Neuron* **86**, 1174–1181 (2015).
95. Berens, P. CircStat : A MATLAB Toolbox for Circular Statistics. *J. Stat. Softw.* **31**, 1–21 (2009).
96. Cagnan, H. *et al.* Temporal evolution of beta bursts in the parkinsonian cortical and basal ganglia network. *Proc. Natl. Acad. Sci.* **116**, 16095–16104 (2019).

97. Schindelin, J. *et al.* Fiji: an open-source platform for biological-image analysis. *Nat. Methods* **9**, 676–682 (2012).